A THESIS SUBMITTED TO
THE GRADUATE SCHOOL OF NATURAL AND APPLIED SCIENCES
OF ÇANKIRI KARATEKIN UNIVERSITY

IMPLEMENTATION AND CONTROL OF WIND TURBINES BASED ON DOUBLY-FED INDUCTION GENERATORS

IN PARTIAL FULFILLMENT OF THE REQUIREMENTS
FOR
THE DEGREE OF MASTER OF SCIENCE
IN
ELECTRICAL AND ELECTRONICS ENGINEERING

BY

ABDULLAH MUWAFAQ OTHMAN ALYOUSUF

ÇANKIRI

2022

IMPLEMENTATION AND CONTROL OF WIND TURBINES BASED ON DOUBLY-FED INDUCTION GENERATORS

By Abdullah Muwafaq Othman ALYOUSUF

July 2022

We certify that we have read this thesis and that in our opinion it is fully adequate, in scope and in quality, as a thesis for the degree of Master of Science

Advisor : Assoc. Prof. Dr. Fatih KORKMAZ

Examining Committee Members:

Chairman : Assoc. Prof. Dr. Nihat DALDAL
Electrical - Electronics Engineering
Bolu Abant İzzet Baysal University

Member : Assoc. Prof. Dr. Fatih KORKMAZ
Electrical - Electronics Engineering
Çankırı Karatekin University

Member : Asst. Prof. Dr. Göksu GÖREL
Electrical - Electronics Engineering
Çankırı Karatekin University

Approved for the Graduate School of Natural and Applied Sciences

Prof. Dr. İbrahim ÇİFTÇİ
Director of Graduate School

I hereby declare that all information in this document has been obtained and presented in accordance with academic rules and ethical conduct. I also declare that, as required by these rules and conduct, I have fully cited and referenced all material and results that are not original to this work.

Abdullah Muwafaq Othman ALYOUSUF

ABSTRACT

IMPLEMENTATION AND CONTROL OF WIND TURBINES BASED ON DOUBLY-FED INDUCTION GENERATORS

Abdullah Muwafaq Othman ALYOUSUF

Master of Science in Electrical - Electronics Engineering

Advisor: Assoc. Prof. Dr. Fatih KORKMAZ

July 2022

In this study, we deal with the MATLAB/Simulink modelling, implementation, and control of wind turbines based on doubly-fed induction generators. in detail, a background of wind blow energy as renewable energy is submitted, while the classification of generators used for a wind turbines are presented. In turn, a preview of doubly-fed induction generators (DFIGs) is presented recalling their advantages and contributions to improving the energy efficiency of wind turbine systems. Also, a comparison between the efficiency of energy of wind turbines which are based on doubly-fed induction generators, and the efficiency of energy of wind turbines which are based on other generators is made. Furthermore, the control process of the doubly-fed induction generators current is evaluated and modelled. Eventually, the investigation of the current controllers is presented.

2022, 89 pages

Keywords: Wind turbines, Doubly-fed induction generators, Current controllers, Energy efficiency, Renewable energy.

ÖZET

ÇİFT BESLEMELI ENDÜKSIYON JENERATÖRLERINE DAYALI RÜZGAR TÜRBINLERININ UYGULANMASI VE KONTROLÜ

Abdullah Muwafaq Othman ALYOUSUF
Elektrik - Elektronik Mühendisliği, Yüksek Lisans
Tez Danışmanı: Doç. Dr. Fatih KORKMAZ
Temmuz 2022

Bu çalışmada, çift beslemeli asenkron jeneratörlere dayalı rüzgar türbinlerinin MATLAB/Simulink tabanlı modellenmesi, uygulanması ve kontrolü ele alınmaktadır. Ayrıntılı olarak, yenilenebilir enerji olarak rüzgar enerjisinin geniş bir arka planı sunulurken, bunun için kullanılan jeneratörlerin bir sınıflandırması yapılmış ve açıklanmıştır. Sırasıyla, rüzgar türbini sistemlerinin enerji verimliliğini artırmadaki avantajlarını ve katkılarını hatırlatan çift beslemeli asenkron jeneratörlerin (ÇBAG) bir genel bakışı sunulmaktadır. Çift beslemeli asenkron jeneratörlere dayalı rüzgar türbinlerinin enerji verimleri ile diğer jeneratörlere dayalı rüzgar türbinlerinin enerji verimlerinin karşılaştırılması yapılmıştır. Ayrıca çift beslemeli asenkron jeneratörlerin akım kontrol süreci değerlendirilmiş ve modellenmiştir. Son olarak, mevcut kontrolörlerin incelenmesi sunulmuştur.

2022, 89 sayfa

Anahtar Kelimeler: Rüzgar türbinleri, Çift beslemeli asenkron jeneratörler, Akım kontrolörleri, Enerji verimliliği, Yenilenebilir enerji.

PREFACE AND ACKNOWLEDGEMENTS

I would like to thank my thesis advisor, Assoc. Prof. Dr. Fatih KORKMAZ, for his patience, guidance and understanding.

A Thanks to whom, without her, I would not be. Whoever made my life filled with love, I am so grateful to my dear father, mother and brothers for their prayers and constant support.

Last but not least, I am very grateful to Çankırı Karatekin University and all its professors, and everyone who contributed to completing this thesis.

Finally, I would like to thank everyone who has participated in one way or another in giving my letter its current form.

Abdullah Muwafaq Othman ALYOUSUF
Çankırı-2022

CONTENTS

LIST OF SYMBOLS

A_R	Rotor sweeping area
C_D	Drag coefficients
C_L	Lift coefficients
C_p	Performance coefficient
E_R	Induced EMF in the rotor
E_S	Induced EMF in the stator
g_r	Gear Box Ratio
h	Height
h_0	Coefficient of the roughness
I_R	Current of rotor
I_S	Current of stator
J_{in}	Inertia of the wind turbine
L_{GB}	Gear box losses
L_{GS}	Grid side losses
L_{IG}	Inductions generator losses
L_{low}	Losses at low speed of wind
L_M	Mutual inductance
L_R	The inductance of rotor
L_{RS}	Rotor side losses
L_S	Inductance of stator
n_p	Number of Poles
N_R	Rotor number of turns per phase
N_S	Stator number of turns per phase
P_{mec}	Mechanical energy
P_R	Active power of the rotor
P_S	Active power of the stator
Q_R	Reactive power of the rotor
Q_S	Reactive power of the stator
r_R	Radius of the rotor
R_R	Resistance of rotor
R_S	Resistance of stator
s	Slip
T_{eg}	Electro-mechanical torque of generator
T_{em}	Electromagnetic torque
T_R	Rotor torque
T_{sh}	Torque of the shaft
V_R	Supplied voltage of rotor
V_S	Supplied voltage of stator
w	Wind velocity

α	Attack angle
β	Pitch angle
θ_R	Rotor Angle
θ_S	Stator Angle
λ	Ratio of tip speed
ρ	Air density
ϕ	Phase between rotor and stator
ψ_R	Flux of rotor
ψ_S	Flux of stator
ω	Mean wind velocity
ω_{mec}	mechanical velocity
ω_r	Relative wind velocity
ω_r	Rotational velocity
Ω_R	Rotor velocity

LIST OF ABBREVIATIONS

DFIG	Doubly fed induction generator
FSG	Fixed speed generator
PI	Proportional integrator
PLL	Phase locked loop
PMSG	Permanent magnet synchronous generator
RES	Renewable energy resource
VSG	Variable speed generator
WECS	Wind energy conversion system

LIST OF FIGURES

LIST OF TABLES

1. INTRODUCTION

Under the epitome of this thesis, it addresses the implementation and control of doubly-fed induction generators for wind turbines, while the suggested model will be analyzed and simulated in order to compare its efficiency to different generators systems used for a wind turbine.

Through the upcoming sub-titles, a background of wind blow energy as a renewable energy resource (RES) is submitted, while classification of generators used for wind turbine is as follow. In turn, a preview of doubly-fed induction generators (DFIGs) are presented recalling their advantages and contributions in improving the energy efficiency of wind turbine systems. Eventually, this chapter ends with the announcement of the thesis's matter, its purposes, and the organization of its chapters and outlines.

1.1 Background

We would be very certain and accurate when we say that evolution of economy and technology depends essentially on providing energy permanently. This energy is basically obtained from traditional fossil fuel sources, which are not only unsustainable but also damaging environment. Due to the continuous growth of evolution in energy harvesting technologies, these non-renewable resources are being substituted by sustainable environment friendly ones.

These resources "which are clean, available and renewable" are occupying more important place recently because of their enormous contributions in order to create the new generation of energy leaving behind the fossil fuel energy and similar traditional energy resources; therefore, the liberty from fuel energy's dependence would be achieved which pave the way to a "Sustainable World".

The term "Renewable Energy Resources" already exists and many types of these resources have been deployed. It could be harvested from sun as solar energy, from wind by means of turbines, biomass or hydro energy…etc. The wind energy attracts our concern the most and severs our topic essentially, so it would be discussed in detail in the following lines in order to reach the description of our proposal matter related to wind energy.

Wind energy, as renewable sustainable energy resources, is at the top of harvestable energy resources, it has a historical reputation for more than 2500 years old as a clean and free source of energy. However, its fundamental function is to exploit the wind velocity in order to rotate the movable part of a generator, so its fixed part generates the energy. However, the overall installation for producing energy suffers from various issues such as variations of environment, economic obstacles, devices lifetime and alteration of network. These issues are the main reason to perform studies and researches to fulfill the purpose of feasibility estimation, installation costs, controlling and modeling methods, energy system converting and integrating and environmental influences.

The evolution in energy conversion field allows various configurations of Wind-Energy-Conversion-Systems "WECSs" to be achievable; as a result, this evolution creates chances for implementing various designs of generators. These generators can be classified according to fundamental operating and installation methods in many and various categories, but our concern focus on the classification which distinguish between generators depending on fundamental principle of operation; hence it includes two main categories (Geng et al. 2012):

- Fixed Speed Generators "FSG".
- Variable Speed Generators "VSG".

The second one Variable Speed Generators "VSGs" attracts our concern the most, because it serves essentially our topic. Furthermore, one of the most famous and hired generators among the wind turbine energy field "which are classified as VSGs" is the Double Fed Induction Generators "DFIGs".

The strategy of designers and technicians based on achieving and implementing grid demanding and needs was the main pillar for developing this technology which fulfils their desire to maximizing harvested energy, decreasing mechanical capacity and stress. This strategy can become a reality in case of implementing wind turbine based on DFIGs.

1.2 The Matter Announcement

In order to reach more accurate and equivalent reliable mathematical models for DFIG, researches and studies have been performed for proposing analysis and simulation of DFIG's characteristics. Moreover, DFIG's prevalence in wind turbines field increases the absolute necessity of appropriate and adequate model which provide an equivalent performance of DFIG regarding variable networks' conditions.

Considering the above discussion, the main objective of our proposal is to build an equivalent mathematical model which simulates the overall system (i.e., Wind Turbine based on DFIGs). The process starts with building a model for wind turbine, taking into account the mathematical equations and equivalent circuits, while the ultimate model simulates the influence of DFIG on wind turbine behavior considering two principles modes which are Steady-Case mode and Transient-Terms mode. The resultant ultimate model will be analyzed and discussed in order to measure the efficiency of the proposal model, in addition to a comparative study with results belong to already suggested models.

1.3 Purposes and Objectives

According to what has been just discussed; this thesis is intended to achieve the following objectives:

- Describing of characteristics of the wind systems, and also clarifying the transformation of the energy in the wind turbines (mechanical energy) based on various methods.

- Presenting the theoretical concepts of the energy efficiency for wind turbines based on doubly-fed induction generators in the term of electric field.

- Introducing of steady or static case of induction systems methods and also their performance characteristics.

- Introducing and presenting the dynamic case of the induction systems methods. Furthermore, describing the components of the control's vector which belong to doubly-fed induction generators.

- Modeling and evaluating the performance of doubly-fed induction generators regarding various current controllers. Moreover, investigating the doubly-fed induction generators' response.

2. LITERATURE REVIEW

Wind energy is at the top of harvestable energy resources, it has a historical reputation for more than 2500 years old as a clean and free source of energy. However, its fundamental function is to exploit the wind velocity in order to rotate the movable part of a generator, so its fixed part generates the energy.

Over the past few years, wind energy has been growing rapidly all over the world. The wind energy is an important source of renewable energy, which undoubtedly has achieved the highest growth in terms of installed capacity (Mehrjerdi et al., 2021) (Mostafa Nosratabadi et al., 2021). Wind turbines have many advantages that attract a lot of attention due to environmental concerns (Döşoğlu, 2021). Wind turbines have the ability to generate large amounts of energy. It should be noted, however, that the stochastic nature of wind energy alters the electrical energy generated. Therefore, it is more attractive and convenient to extract maximum power from wind by means of maximum power point tracking (MPPT) (Nosratabadi et al., 2021). There are several types of wind energy conversion methods. In the wind farm industry, the concept of variable speed wind turbines has received more attention because it is more controllable, more efficient and has good power quality(Gebru et al., 2020).

The evolution in energy conversion field allows various configurations of Wind-Energy-Conversion-Systems “WECSs” to be achievable; as a result, this evolution creates chances for implementing various designs of generators. These generators can be classified according to fundamental operation and installation methods in many and various categories; hence it includes two main categories: Fixed Speed Generators “FSG” and Variable Speed Generators “VSGs”(Geng et al. 2012).

The second one Variable Speed Generators “VSGs” attracts the concern the most because of their advantages and powerful points; especially that it is adopted widely in the energy and economic field (Burton et al. 2001). Manufactures and industrial companies are moving towards building and development of wind turbines with higher energy, which could reach to 6 MW (Ackermann and Söder 2002). This range of energy can be created by adopting VSGs wind turbines, where the pitch can be controlled by adopting synchronous generators, or by adopting doubly fed induction generators. In contrast, the fixed-speed induction ones are considered as unfeasible regarding the development of wind turbines with higher energy.

Furthermore, one of the most famous and hired generators among the wind turbine energy field “which are classified as VSGs” is the Double Fed Induction Generators “DFIGs”. These types of generators have a very important advantage that the energy electronic system has to operate at a fraction up to 30% of the overall energy of the system.

The wind turbines based on doubly fed induction generators “DFIG” has a powerful point that the energy electronic system has to deal with a range of fraction from 20% up to 32% of the overall energy of the system. This advantage points to reduction of the waste in the energy of the electronic system and save more energy (Hansen et al. 2001), (Morel et al. 1998) and (Xu and Cheng 1995).

A comparative study for the generated energy between various configurations of wind turbines has been performed in Datta and Ranganathan (2002). This comparative study includes (i) the fixed-speed configuration, (ii) variable speed adopting induction generators configuration and (iii) full variable speed adopting doubly fed induction generators configuration.

The energy generated by wind turbines based on variable speed generators can be 2% and reach 6%, if this energy is compared to that generated by wind turbines based on fixed speed generators (Carlson et al. 1996). While the thesis in Zinger and Muljadi (1997) has indicated that the energy could reach 40%. In the same context, the comparison between wind turbines generators showed that the gain (i.e., the output energy relative to the input) in produced energy by variable speed generators start at 3% and reach up to 30% (comparing to variable speed ones) regarding the influence of the case circumstance and design factors.

The efficiency of the energy produced by doubly fed induction generators has been introduced and presented in Ioannides and Tegopoulos (1988) and Rabelo and Hoffman. (2001). While in Tang and Xu (1995) the computations and the mathematical concepts of the energy efficiency produced by doubly fed induction generators are introduced and presented. Furthermore, the thesis in Datta and Ranganathan (2002) the comparison of energy produced by wind turbines based on various designs and configurations has been performed. These designs and configurations are:

- Wind turbines based on fixed speed adopting induction generators. Even though it is known as fixed speed generators, but the speed actually vibrates within 1% of the nominal value, so the speed of rotor is almost fixed or any way rather fixed (Papadopoulos 1999).
- Wind Turbines systems based on Variable Speed integrated with multiple poles generators which could be either Permanent Magnet Synchronous generators (PMSGs) or synchronous ones.
- Wind turbines based on full variable speed adopting doubly fed induction generators.

The energy produced by wind turbines based on doubly fed induction generators is greater than that energy produced by wind turbines based on fixed speed adopting induction generators. This method has been adopted and considered widely over the last decades in different systems and applications in order to provide energy within a range of Mega-Watts. These systems based on Doubly Fed Induction Generator (DFIGs) have been manufactured and tested by various companies such as Nordex and Dewind.

The energy produced by wind turbines based on doubly fed induction generators could reach over than 60% comparing with fixed speed induction generators configurations. Considering the variable speed generators equipped with cage rotor induction, this produced energy could reach over than 20%. It is noteworthy that the thesis in Datta and Ranganathan (2002) has ignored or disregarded parameters and aspects like:

- Distribution of wind.

- Waste caused by mechanical fraction.
- Waste caused electrical components.

Despite of neglecting not only the mechanical losses but also the electrical ones, we will take them into consideration during the calculations. On the other hand, the generated electrical power calculations are based on special cases for wind turbines and related to average velocity equal to 10 meter per second.

The generated electrical power is significantly improved by adopting DFIG method and can reach more than 20% in order to compare it to the generated electrical power which his produced by variable speed induction generator method. This significant improvement and enhancement in produced power refers probably to the fact that in the variable speed induction generator method, the generator is operating in the inefficiently for high values of wind speeds.

The complexity of controlling of the wind turbines based on variable speed adopting doubly fed induction generators is greater than controlling wind turbines based on typical induction generators. Furthermore, the first controlling procedure includes the same restrictions and constrains that the controlling procedure of synchronous machines have (Leonhard 2001).

The simulations have indicated that the variations in load and changes of stator energy have a huge influence on the flux (Wang and Ding 1993). They showed that the oscillation of flux happens strictly in the case of higher velocity comparing with the oscillation of flux at smaller values of velocity. In addition, the thesis in Heller and Schumacher (1997) has announced the investigation that doubly fed induction generators is stable and steady depending on mathematical equations. It has clarified that the dynamic of these generators has slightly damped Eigen-values respecting the natural frequency while the machine is unsteady at specific working cases. The aforementioned slightly damped has a huge influence on the current of rotor (i.e., the EMF). Considering the analysis and evaluating of the execution of various current controlling methods, there is no thesis or any related research has done that analysis or evaluating regarding the elimination of the EMF impact in the current of rotor.

The execution or performance of doubly fed induction generators regarding the disturbances of grid is scarcely handled by related thesis and literature. Furthermore, we can say that it is barely addressed or treated. Except the thesis of Johnson (1985) which concentrated on damping's quality and the speed of the damping in the disturbances of grid. In contrast, many parameters and aspects related to the rotor current have been ignored like:

- Bandwidth of controlling loops' current.
- Disturbances' size of the grid.

3. WIND CHARACTERISTICS

In the following titles, the wind's characteristics will be presented and described. Wind's properties, distribution, turbulence and simulation are described in the theorem and by the mathematical relations and formulas. Moreover, the second section is addressed to the conversion of the aerodynamic related to the wind. The control of power and the C_p curve are presented and described.

3.1 Wind's Properties

One of the most important wind characteristics is the wind's properties. These properties attract our concern the most while they are related essentially to the topic of our thesis.

The first sub-title of this section will be addressed to the wind's distribution which is related to describe the probability of an indicated mean of wind velocity, and also to calculate certain parameters or factors such as generated power. In contrast, the second sub-title of this section will be addressed to the wind's turbulence which is related to the variations of wind velocity.

3.1.1 Wind's distribution

the wind's distribution is referred to the probability of an indicated mean of wind velocity. This mean velocity is usually measured by the mean per year (or annual mean). This parameter or factor (i.e., the annual mean) is a very essential factor for determine the produced energy by a wind turbine. Moreover, the wind velocity could be indicated per a day or month or any period of time. Even though, it depends on the annual mean and the distribution of the wind. In order to describe the formula of the mean wind velocity, we have to present and mention first some mathematical relations and definitions related to probability (Liserre et al. 2011).

If we define a continuous random parameter (let be X) which has the Weibull distribution as a probability density function, then we can describe the probability of X is equal to a value x as Equation (3.1),

$$g(X = x) = k.\frac{x^{k-1}}{c^k}.\exp\left(-\left(\frac{x}{c}\right)^k\right) \quad (3.1)$$

Where: k, c are the shape and scale factors. Thus, the expectation of X can be described as Equation (3.2),

$$E(X = x) = \int x.g(X = x)dx = \int k.\frac{x^k}{c^k}.\exp\left(-\left(\frac{x}{c}\right)^k\right)dx = \frac{c}{k}.\ \Gamma(k^{-1}) \quad (3.2)$$

Where Γ is the Gamma function which its formula is given Equation (3.3),

$$\Gamma(k) = \int_0^\infty x^{k-1}.\exp(-x)\,dx \quad (3.3)$$

Let be that continuous random parameter is the wind velocity w which has the Weibull distribution as a probability density function, and then we have Equation (3.4),

$$g(w) = k.\frac{w^{k-1}}{c^k}.\exp\left(-\left(\frac{w}{c}\right)^k\right) \quad (3.4)$$

Thus, the mean wind velocity $\overline{w}$ (or the predicted wind velocity) is equal to the expectation of w, as Equation (3.5),

$$\overline{w} = E(X = w) = \int w.g(X = w)dw = \frac{c}{k}.\ \Gamma(k^{-1}) \quad (3.5)$$

A very special case of the previous density function (Weibull distribution) is the Rayleigh distribution when the parameter of shape is equal to 2 ($k = 2$) (Johnson 1985). Thus, the probability density function of the wind velocity and the mean wind velocity $\overline{w}$ become as given Equation (3.6) and Equation (3.7),:

$$g(w) = 2.\frac{w}{c^k}.\exp\left(-\left(\frac{w}{c}\right)^2\right) \tag{3.6}$$

$$\overline{w} = \frac{c}{2}.\ \Gamma(0.5) \tag{3.7}$$

The following Figure 3.1 illustrates the probability density function of the wind velocity (Rayleigh case). For a given $\overline{w}$, we can calculate the scale factor from the relation as given Equation (3.8):

$$k = 2\,,\ \ \Gamma(0.5) = \sqrt{\pi}\ \ \rightarrow\ \ c = \frac{2}{\sqrt{\pi}}.\overline{w} \tag{3.8}$$

For the large values of the wind velocity ($w > 15\ m/s$), we can see that the probability density function is limited to zero. For example, in the curve No. 1, the mean wind velocity is equal to 5.5 m/s.

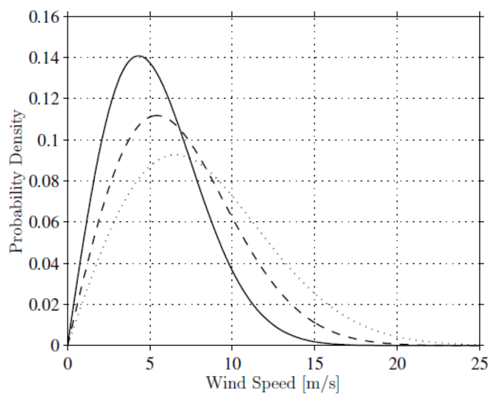

Figure 3.1 Probability density function of the wind velocity (Petersson 2005)

3.1.2 Wind's turbulence

This concept refers to the variations or changes of wind velocity. These changes act continuously for shorter periods of time. In order to model and compute the wind velocity in this case, we have to adopt a spectral density function which is related to the turbulence. Speaking of which, these are many spectral density functions which could be used such as von Karman function, Frost function (Liserre et al. 2011)] (Veers 1988).

One of the most famous spectral density functions is known as Kaimal function (Veers 1988), which is given by the Equation (3.9) in terms of frequency f:

$$L(f) = \frac{0.16}{ln^2\left(\frac{h}{h_0}\right)} \cdot \frac{105.h.\overline{w}_0}{(1+33.\frac{h.f}{\overline{w}_0})^{5/3}} \tag{3.9}$$

Where L is the longitudinal speed component of the spectrum, h is the height, h_0 is the coefficient of the roughness and $\overline{w}_0$ is the mean wind speed at h_0.

Considering the changes of wind velocity dimensions, the wind velocity changes in 3 dimensions. Therefore, the method Sandia has been developed in order to simulate and compute the variation of wind velocity in the space (Veers 1988), (Winkelaar 1991).

3.2 Conversion of Aerodynamic

During the air flow over a blade of surface, the blade is affected by two forces; the first one, which is the drag force D, acts in a direction parallel to the flow. While the second one, which is the lift force L, acts in a direction perpendicular to the flow.in addition, we define the angle measured between the flow direction and the blade's chord line as the attack angle α. In contrast, we define the angle measured between the rotating plane and the blade's chord line as the pitch angle β (Johnson, 1985). The following Figure 3.2 illustrate the aforementioned definitions of angles.

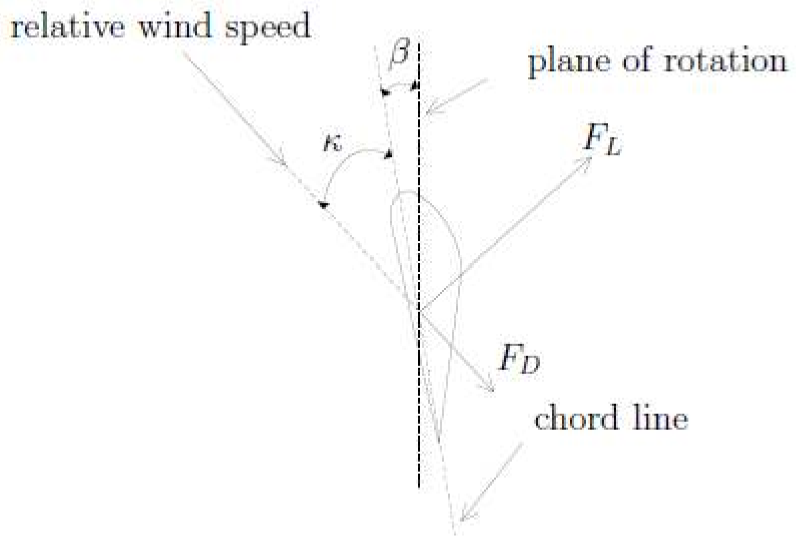

Figure 3.2 Definitions of angles and forces (Petersson 2005)

In a case when α is greater than certain value, we can see that the drag force increases, while the lift force decreases until the flow around the blade stalls (i.e., the lift force is too small and inactive) (Burton et al. 2001).

Equation (3.10) and Equation (3.11) give the derivative of drag force dD and lift force dL according to span length changes dx (Spera 1994):

$$\frac{dD}{dx} = \frac{1}{2}.\rho.c.C_D.w_r^2 \tag{3.10}$$

$$\frac{dL}{dx} = \frac{1}{2}.\rho.c.C_L.w_r^2 \tag{3.11}$$

Where ρ is the air density, c is the chord line length, w_r is the relative wind velocity and C_D, C_L are the drag and lift coefficients respectively. These last two coefficients are usually defined in terms of the attack angle α as shown in the Figure 3.3.

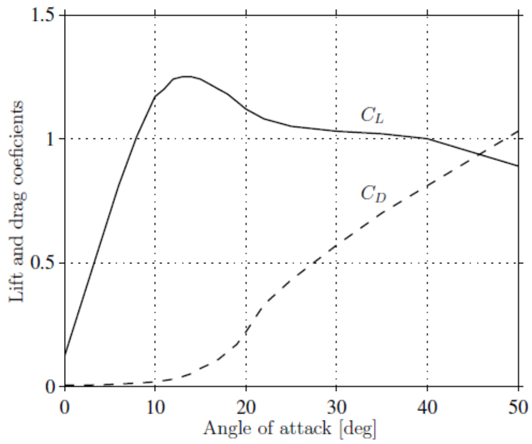

Figure 3.3 Drag and lift coefficients in terms of the attack angle (Petersson 2005)

3.2.1 Power control methods

The main purpose of the controlling process is to obtain the required amount from the power produced by wind speeds. But in the case of high speeds of wind, the power produced by wind speeds has to be limited. In the same context, we can basically classify the power control in 3 methods, as follows:

- Active stall method.
- Stall method.
- Pitch method.

The first two methods imply that the affected surface is meant to be in a stall situation at high speeds of wind; therefore, the system requires no control in pitch angle. While considering the last method which is the most known and widespread one for controlling the power produced by the wind turbines, especially the larger ones. This method is widely adopted for wind turbines based variable speed generators. The two-principle cinereous in the pitch control method are as follows (Burton et al. 2001):

- First cinereous: The wind speed is smaller than the rate, so the produced power by wind turbine has to be as much as possible. In this case, the harvested power is maximized by controlling the pitch angle.

- Second cinereous: The wind speed is greater than the rate, so the produced power is limited at its range. In this case, the harvested power is limited by controlling the pitch angle in order to reduce the attack angle, or to increase it towards the stall situation which in turns limits the power.

3.2.2 Performance coefficient C_p

The power that is harvested from the wind turbines usually described as percentage of the overall power which is in turns given in terms of a coefficient known as the performance coefficient C_p. However, depending on theoretical manners or measuring manners, this coefficient C_p can be computed or calculated (Burton et al. 2001). normally, the coefficient C_p is described as a function of the pitch angle β and the ratio of tip speed λ, so it is written usually as $C_p(\beta, \lambda)$. The ratio λ is determined by the following Equation (3.12) (Johnson 1985):

$$\lambda = \frac{\Omega_R}{w} r_R \tag{3.12}$$

Where w is the wind velocity, r_R the radius of the rotor and Ω_R is rotor velocity. For a certain value of pitch angle β, the following Figure 3.4 illustrates the coefficient $C_p(\lambda)$ in terms of the ratio of tip speed λ:

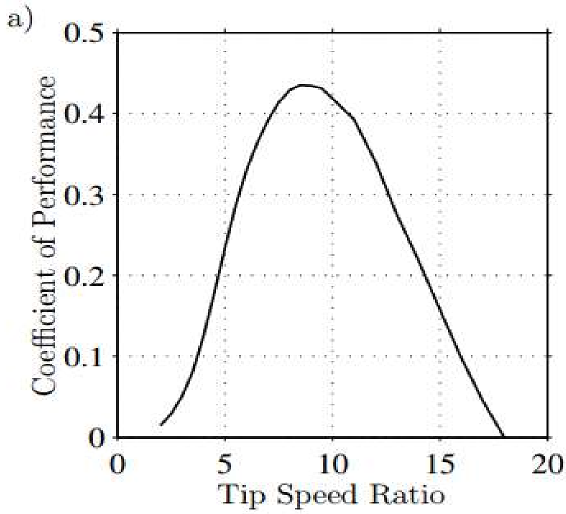

Figure 3.4 The coefficient $C_p(\lambda)$ in terms of the ratio of tip speed (Abad *et al.* 2011)

Considering the steady case of the mechanical energy produced by wind turbines, the performance coefficient C_p method is used in order to calculate the mechanical energy in the steady case. Moreover, this method is known as the C_p curve method. The following Equation (3.13) gives the mechanical energy P_{mec} produced by wind turbines in terms of performance coefficient C_p (Johnson 1985):

$$P_{mec} = \frac{1}{2}.(\rho. A_R. w^3).C_p(\beta, \lambda) \tag{3.13}$$

Where ρ is the density of air, β is the pitch angle, λ is the ratio of tip speed, w is the wind velocity, A_R is the rotor sweeping area and $C_p(\beta, \lambda)$ is performance coefficient. For a rated rotor velocity Ω_R, the following Figure 3.5 illustrates the mechanical energy P_{mec} in terms of the wind velocity w.

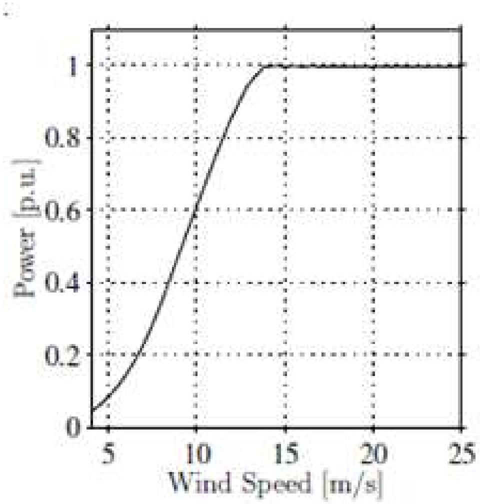

Figure 3.5 Mechanical energy $\boldsymbol{P_{mec}}$ in terms of the wind velocity **w** (Pena *et al*., 1996)

The theoretical value of the coefficient $C_p(\beta,\lambda)$ based on the Betz limit can be calculated as given Equation (3.14):

$$C_p(\beta,\lambda) = 0.59 \tag{3.14}$$

The following Figure 3.6 illustrates the different cases for C_p related to wind turbine of three blades. In addition, it shows the effect of the parameter β on the coefficient C_p.

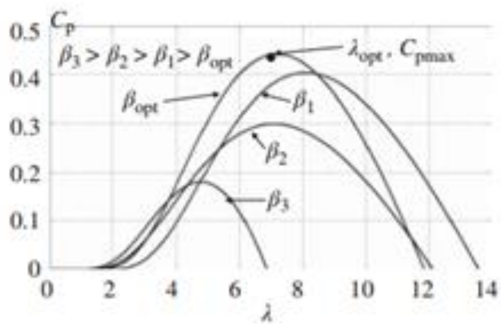

Figure 3.6 Different cases for $\boldsymbol{C_p}$ related to turbine of three blades (Pena *et al.*, 1996)

Speaking of mechanical energy and regarding the wind turbine based on variable speed, we show the variation of mechanical energy P_{mec} in terms of changes in wind velocity w

Figure 3.5. In the same context, the Figure 3.7 shows the variation of rotor velocity Ω_R in terms of changes in wind velocity w, as we can see that the relation is linear in the variable speed section.

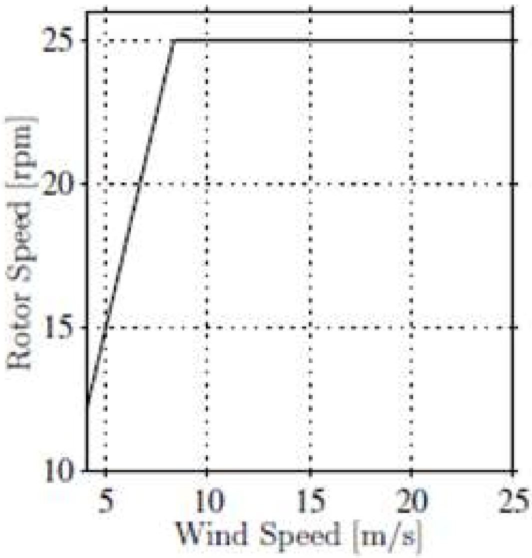

Figure 3.7 Variation of rotor velocity in terms of changes in wind velocity (Petersson 2005)

For the rotor velocity Ω_R and regarding the variable speed section, the control process focusses on controlling the rotor velocity in order to obtain the optimum value of the ratio λ. Consequently, the performance coefficient $C_p(\lambda)$ has to be at the maximum value unless the either the rotor velocity Ω_R or the energy is above its range. In contrast, we can see when the rotor velocity Ω_R or mechanical energy P_{mec} reaches the rate, the harvested power is limited by controlling the pitch angle (Liserre *et al.* 2011).

Considering the Figure 3.5 and Figure 3.7, we can observe that the wind turbine has reached its rated energy P_{mec} at an approximate value of wind velocity $w = m/s$, while it has reached its rated rotor velocity Ω_R at an approximate value of wind velocity $w = m/s$.

In the light of the previous study, we can write Equation (3.15),

$$A_R = 2.\frac{P_{mec}}{\rho.w^3.C_p(\beta,\lambda)} = f(r_R) \quad (3.15)$$

We can see that the rotor sweeping area A_R is a function of the radius of the rotor r_R. On the other hand, the relationship between the radius r_R and the energy P_{mec} is a proportional relationship (i.e., when the radius r_R a decrease, the energy is also decreases, and vice versa). Consequently, we can determinate the design of the wind turbine system which gives us the optimal values of the radius r_R of the rotor according to various values for wind velocity w. Even though, the design process is bounded by two constrains. The first one is that decreasing the radius r_R significantly will imply the energy to reach its rate very fast and at slower wind velocities. While the second one is that increasing the radius r_R significantly will force the pitch control to limit the energy. Consequently, the design process has to verify a balance between harvested energy and the radius of rotor r_R regarding the mean wind velocity w of the location.

3.3 Rotor Speed Control

The evolution in energy conversion field allows various configurations of Wind-Energy-Conversion-Systems to be achievable; as a result, this evolution creates chances for implementing various designs of generators. These generators can be classified according to fundamental operating and installation methods in many and various categories, but our concern focus on the classification which distinguish between generators depending on ability of controlling the speed of rotor; hence it includes two main categories:

- Fixed Speed Generators “FSG”.
- Variable Speed Generators “VSG”.

For the wind turbine based on the first category (i.e., fixed speed), the generators and the grid are linked in a direct way. Even though it is known as fixed speed generators, but the speed actually vibrates within 1% of the nominal value, so the speed of rotor is almost fixed or any way rather fixed. Consequently, the speed isn’t able to be controlled and the energy produced by the wind turbulence isn't storable. As a result, the wind turbulence will affect the energy's stability and constancy (Papadopoulos, 1999).

For the wind turbine based on the second category (i.e., variable speed), the operation principle is based on controlling the speed of rotor, which lead to increase or decrease the fluctuations of the energy according to the speed of rotor. These fluctuations happen because of the changes of energy. One of the most advantages of the variable speed method that the energy's stability and quality are able to be enhanced and optimized comparing to the previous method (the fixed speed) (Larsson *et al.* 1999) (Petru and Thiringer 2000).

3.4 The Rotational Velocity

Considering the adjustment and correspondence between the rotational velocity ω_r of the wind turbines and the frequency of the electrical grid. This adjustment or correspondence is achievable by adopting on of the following ways:

- Gear Box Ratio g_r adjustment.
- Number of Poles n_p adjustment, which indicate the mechanical velocity ω_{mec}.

Hence the rotor velocity Ω_R ,which is correspondent to the electrical frequency, is:

$$\omega_r = (n_p . g_r) . \Omega_R \quad (3.16)$$

$$\frac{d\omega_r}{dt} = (n_p . g_r) \frac{d\Omega_{RT}}{dt} \quad (3.17)$$

where in Equation (3.16) and Equation (3.17), Ω_R is the correspondent rotor velocity, ω_r is the rotational velocity, n_p is the number of poles and g_r is the gear box ratio. In context, the mechanical velocity ω_{mec} ca be expressed in terms of the rotational velocity ω_r as follows in Equation (3.18) and Equation (3.19):

$$\omega_r = n_p.\omega_{mec} \tag{3.18}$$

$$\frac{d\omega_r}{dt} = n_p.\frac{d\omega_{mec}}{dt} \tag{3.19}$$

Consequently, the drive train in the dynamic situation can be described as Equation (3.20) and Equation (3.21):

$$J_g.\frac{d\omega_r}{dt} = J_g.n_p.\frac{d\omega_{mec}}{dt} \tag{3.20}$$

$$J_g.\frac{d\omega_{mec}}{dt} = \frac{J_g}{n_p}.\frac{d\omega_r}{dt} = T_{eg} - T_{sh} \tag{3.21}$$

Where J_g the inertia of the generator is, T_{eg} is the electro-mechanical torque which generator produces and T_{sh} is the torque of the shaft. Back to the rotational velocity ω_r, the drive train in the dynamic situation can be described with Equation (3.22):

$$J_{in}.\frac{d\omega_r}{dt} = T_{sh} - T_R \tag{3.22}$$

Where J_{in} is the inertia of the wind turbine, T_R is the torque which the rotor produces. Replacing the rotor velocity Ω_{RT} in the last equation, thus we have Equation (3.23):

$$\frac{J_{in}}{n_p.g_r}.\frac{d\Omega_R}{dt} = T_{sh} - T_R \tag{3.23}$$

Considering the definition of the angular velocity which indicate that it is equal to the changes of the angle with time, we can express the velocities Ω_{RT} and Ω_R as Equation (3.24) and Equation (3.25):

$$\Omega_R = \frac{d\theta_{RT}}{dt} \tag{3.24}$$

$$\Omega_R = \frac{d\theta_R}{dt} \tag{3.25}$$

Hence, we can express the formula of the torque of the shaft T_{sh} in terms of the angles θ and Ω as Equation (3.26) and Equation (3.27):

$$T_{sh} = \Delta\theta.\gamma + \Delta\Omega.\varepsilon \quad (3.26)$$

$$T_{sh} = (\theta_R - \theta_{RT}).\gamma + (\Omega_R - \Omega_{RT}).\varepsilon \quad (3.27)$$

where γ and ε is the stiffness and the damping coefficients of the shaft.

3.5 Wind Turbines Methods

In this very section, we are presenting the most famous adopted methods in the Wind Turbines systems (Hansen et al. 2001):

- Wind Turbines systems based on Fixed Speed integrated with induction generators.
- Wind Turbines systems based on Variable Speed integrated with either synchronous or induction generators.
- Wind Turbines systems based on Variable Speed integrated with multiple poles generators which could be either Permanent Magnet Synchronous generators (PMSGs) or synchronous ones.
- Wind Turbines systems based on Variable Speed integrated with doubly fed induction generators (DFIGs). This method attracts our concern the most, because it serves essentially our topic.

3.5.1 Fixed speed wind turbines systems

For the wind turbine based on Fixed Speed, the generators and the grid are linked in a direct way as shown in the Figure 3.8. Even though it is known as fixed speed generators, but the speed actually vibrates within 1% of the nominal value, so the speed of rotor is almost fixed or any way rather fixed (Papadopoulos 1999).

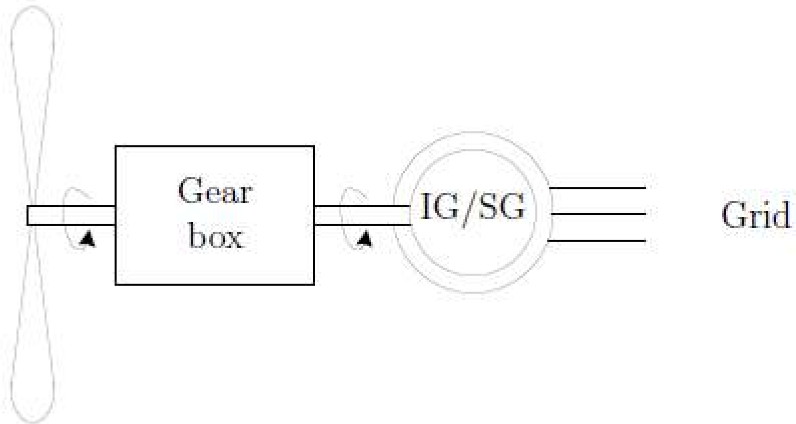

Figure 3.8 Fixed speed wind turbines systems (Petersson 2005)

According to this method, the adjustment and correspondence between the rotational velocity ω_r and the frequency is achievable by adopting the following ways:

- Gear Box Ratio g_r adjustment.
- Number of polar pair adjustment, which indicate the mechanical velocity ω_{mec}.

In addition, double induction generators are added. The first one addresses the low velocities of wind and the other one address the high velocities of wind. This method was the most adopted suitable one in the 80s and 90s of the last centuries (Hansen et al. 2001).

3.5.2 Variable speed wind turbines systems

The Wind Turbine System based on Variable Speed, which is illustrated in the following Figure 3.9, has a generator's stator that is attached to inverter.

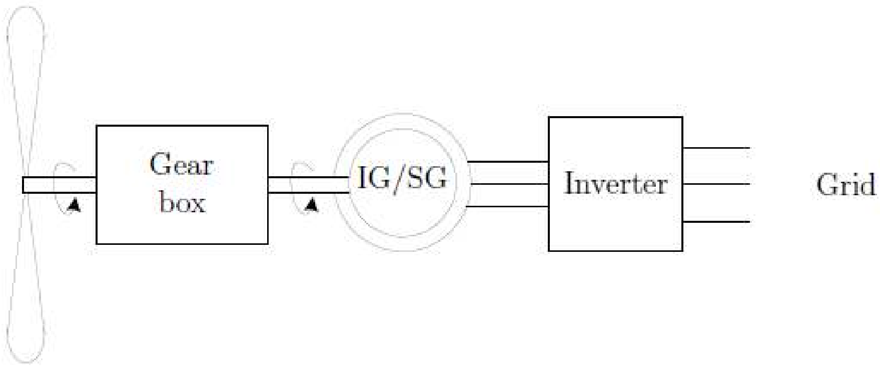

Figure 3.9 Variable speed wind turbines systems (Petersson 2005)

The characteristics of this method are:

- A stand-alone fed induction generator or a synchronous one is implanted.
- The gear box ratio is adjusted to provide the rotor velocity at maximum value in term of the generator’s rated velocity.
- The most important advantage is the stable robust controlling because of the equipped converter (Boldea and Nasar 2016), (Harnefors 2002), (Leonhard 2001).

3.5.3 Variable speed systems integrated with multiple poles generators

The Wind Turbine System based on Variable Speed can be implemented depending one multiple poles generator, which is illustrated in the following Figure 3.10.

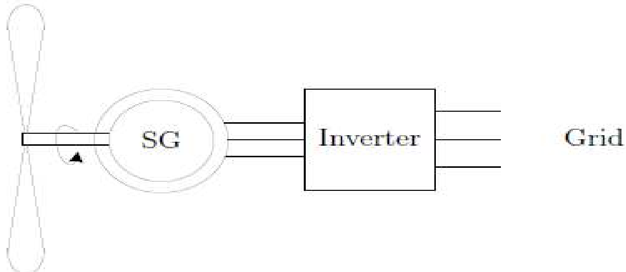

Figure 3.10 Variable speed systems integrated with multiple poles generators (Petersson 2005)

We can observe that the gear box is eliminated in this method. According to Hansen et al. (2001), Enercon has manufactured and tested this implementation for the first time.

3.5.4 Wind turbines based on doubly fed induction generators (DFIGs)

The Wind Turbine System based on Doubly Fed Induction Generator (DFIGs) which is equivalent to constant frequency generator. This method is illustrated in the following Figure 3.11. This method has been adopted and considered widely over the last decades in different systems and applications in order to provide energy within a range of Mega-Watts. These systems based on Doubly Fed Induction Generator (DFIGs) have been manufactured and tested by various companies such as Nordex and Dewind ,(Qiao and Harley 2008).

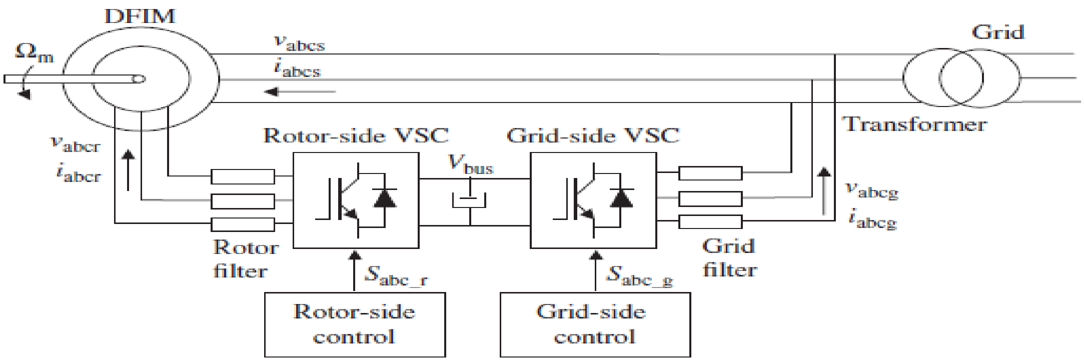

Figure 3.11 Wind Turbines based on Doubly Fed Induction Generator (DFIGs) (Abad et al. 2011) (Petersson 2005)

The DFIGs are more suitable choice for applications with limited velocity, which provide a possibility for reducing the size of converter. In this method, we can observe from the configuration that the generator's stator is directly linked to the grid and also operates at stable frequency and amplitude which produce the magnetic field. In addition, the rotor and stator are equipped by 3 phases voltage which allow a possibility of taking various values for frequency and amplitude in case of steady state (Qiao and Harley 2008). Consequently, various operating cases can be reached, such as required velocity or desired torque, especially by adopting backward-to-backward 3 phases converter as shown in the previous figure (Abad et al. 2011), (Pena et al. 1996). However, more details related to working principles and implementation will be described in the upcoming sections.

4. COMPARISON OF ENERGY EFFICIENCY OF WIND TURBINES

In this section of our thesis, we are presenting a comparative study between various methods of wind turbines which has been mentioned and described in the previous sections. We are assuming here that for all wind turbines methods, the systems are equipped and integrated with mechanism for controlling pitch angle and velocity.

- Wind Turbines systems based on Fixed Speed integrated with induction generators. This configuration is usually equipped with double induction generators are added. The first one addresses the low velocities of wind and the other one address the high velocities of wind.
- Wind Turbines systems based on Variable Speed integrated with either synchronous or induction generators. The characteristics of this method according to, Boldea and Nasar (2016), Harnefors (2002) and Leonhard (2001) are: (i) A stand-alone fed induction generator or a synchronous one is implanted. (ii) The gear box ratio is adjusted to provide the rotor velocity at maximum value in term of the generator's rated velocity. (iii) The most important advantage is the stable robust controlling because of the equipped converter.
- Wind Turbines systems based on Variable Speed integrated with multiple poles generators which could be either Permanent Magnet Synchronous generators (PMSGs) or synchronous ones.
- Wind Turbines systems based on Variable Speed integrated with doubly fed induction generators (DFIGs). In this method, the generator's stator is directly linked to the grid and also operates at stable frequency and amplitude which produce the magnetic field. In addition, the rotor and stator are equipped by 3 phases voltage which allow a possibility of taking various values for frequency and amplitude in case of steady state.

A comparative study for the generated energy between various configurations of wind turbines has been done in (Datta and Ranganathan 2002). This comparative study includes (i) the fixed-speed configuration, (ii) variable speed adopting induction generators configuration and (iii) full variable speed adopting doubly fed induction generators configuration.

Despite of neglecting not only the mechanical losses but also the electrical ones in Datta and Ranganathan (2002), we will take them into consideration during the calculations. On the other hand, the generated electrical power calculations are based on special cases for wind turbines and related to average velocity equal to 10 meter per second. However, we will take into consideration all wind velocities, while the normalization will be done depending on the distribution of wind velocity. The generated electrical power is significantly improved by adopting DFIG method and can reach more than 20% in order to compare it to the generated electrical power which his produced by variable speed induction generator method Abu-Rub et al. (2014), Datta and Ranganathan (2002),. This significant improvement and enhancement in produced power refers probably to the fact that in the variable speed induction generator method, the generator is operating in the inefficiently for high values of wind speeds (Abu-Rub et al. 2014) (Datta and Ranganathan 2002),.

During this study we are arranging here the initial conditions which the calculations and the derived relations are based on:

- The electrical and mechanical losses are taken into consideration during the calculations.
- All wind velocities are taken into consideration. furthermore, the study is compatible with the general case (no special cases are assumed).
- We are neglecting the effect of the turbulence.
- We are neglecting the losses caused by the friction of the slip-rings.

4.1 Overall System Losses

We are describing here the losses which are related to various elements in the wind turbines. I, and for the whole system, these losses will be Concluded and calculated.

In order to calculate the overall system losses, we have to consider the losses caused by the gear box, inductions generator, grid side and finally rotor side. Consequently, the overall system losses are described in the following Equation (4.1):

$$L_{total} = L_{GB} + L_{IG} + L_{GS} + L_{RS} \tag{4.1}$$

Where L_{total} are the overall system losses, L_{GB} is the gear box losses, L_{IG} is the inductions generator losses, L_{GS} is the grid side losses and L_{RS} is the rotor side losses.

Let be the generated power P (as a function to wind velocity w, i.e.,$P(w)$) as a continuous random parameter which has the Rayleigh distribution (A very special case of the density Weibull distribution, where the parameter of shape is equal to 2 ($k = 2$)) as a probability density function, and then we have Equation (4.2):

$$g(w) = 2.\frac{w}{c^k}.exp\left(-\left(\frac{w}{c}\right)^2\right) \tag{4.2}$$

Thus, the mean generated power $\bar{P}$ (or the predicted generated power) is equal to the expectation of P, which given Equation (4.3):

$$\bar{P} = E(P) = \int P(w).g(w)dw \tag{4.3}$$

In addition, the losses caused by the gear box can be estimated and described according to Mutschler and Hoffmann (2002) and Petersson (2005b) as in the following Equation (4.4):

$$L_{GB} = \alpha . L_{low} + \beta \, L_n . \frac{\omega_r}{\omega_{rn}} \tag{4.4}$$

Where ω_r is the rotational velocity, L_{low} is the losses at low speed of wind, α is the losses coefficient related to gear mesh and β is the friction coefficient. However, the values of α and β are indicated for 1 Megawatt gear box as 0.02 and 0.005 respectively (Mutschler and Hoffmann 2002), (Petersson 2005b).

5. DOUBLY FED INDUCTION GENERATOR

The detailed information about Doubly Fed Induction Generators, has been represented in this section.

5.1 Structure and Configuration

The Wind Turbine System based on Doubly Fed Induction Generator (DFIGs) which is equivalent to constant frequency generator. This method is illustrated in the following Figure 5.1. This method has been adopted and considered widely over the last decades in different systems and applications in order to provide energy within a range of Mega-Watts. These systems based on Doubly Fed Induction Generator (DFIGs) have been manufactured and tested by various companies such as Nordex and Dewind .

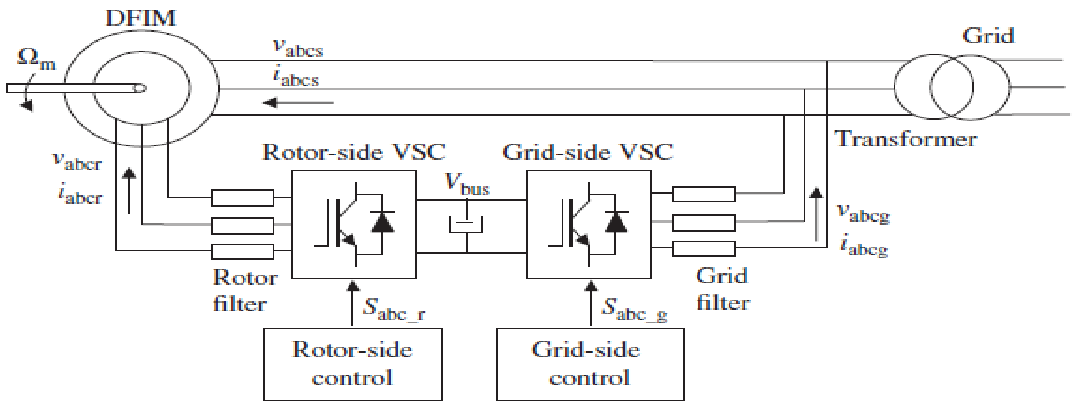

Figure 5.1 Wind turbine system based on DFIGs (Abad et al. 2011)

The DFIGs are more suitable choice for applications with limited velocity, which provide a possibility for reducing the size of converter. In this method, we can observe from the configuration that the generator’s stator is directly linked to the grid and also operates at stable frequency and amplitude which produce the magnetic field. In addition, the rotor and stator are equipped by 3 phases of voltage which allow a possibility of taking various values for frequency and amplitude in case of steady state. Consequently, various operating cases can be reached, such as required velocity or desired torque, especially by adopting backward-to-backward 3 phases converter as shown in the previous figure,.

However, more details related to working principles and implementation will be described in the upcoming sections.

5.2 Steady-State Case

5.2.1 Equations and equivalent circuit

The various frequencies related to the generator are linked together through the following Equation (5.1) (Abad et al. 2011):

$$\omega_R + \Omega_R = \omega_S \tag{5.1}$$

Where ω_R the frequency is related to the rotor, ω_S is the frequency related to the stator and Ω_R is the rotor velocity.

while the shaft's mechanical velocity Ω_M is linked to rotor velocity Ω_R with the number of poles pairs of the generator. This relation can be described as Equation (5.2):

$$\Omega_R = p.\Omega_M \tag{5.2}$$

Consequently, we can define the generator's slip s as Equation (5.3):

$$s = \frac{\omega_R}{\omega_S} = \frac{\omega_S - \Omega_R}{\omega_S} \tag{5.3}$$

where all the previous equations are represented in revolution per minute (rev/min) or in Hertz (Hz) or in radian per second (rad/s).

Among the majority of applications, the stator frequency ω_S (or as it is known the synchronous frequency) is considered as a constant parameter as long as the stator windings are linked to the grid in a direct way. On the other hand, the rotor frequency ω_R

is related to Ω_M the shaft's mechanical velocity, as a result we have three modes of operation according to the velocities or the value of the slip s.

When the rotor velocity Ω_R is greater than ω_S the stator frequency, then we have a negative value of the slip s. The compatible operation mode is Hyper-synchronous mode. While when Ω_R is smaller than ω_S, then we have a positive value of the slip s. The compatible operation mode here is Sub-synchronous mode. Eventually, when Ω_R is equal to ω_S, then we have a zero value of the slip s. The compatible operation mode here is synchronous mode. We summarize the previous operations modes as follows:

$$\Omega_R > \omega_S \quad => \quad \omega_R < 0 \quad => \quad s < 0 \quad => \quad \text{Hyper} - \text{synchronous mode}$$

$$\Omega_R < \omega_S \quad => \quad \omega_R > 0 \quad => \quad s > 0 \quad => \quad \text{Sub} - \text{synchronous mode}$$

$$\Omega_R = \omega_S \quad => \quad \omega_R = 0 \quad => \quad s = 0 \quad => \quad S\text{ynchronous mode}$$

In order to derive the equivalent circuit which models the steady state of a DFIGs system, we have to consider the following assumptions:

- The idealization condition is considered. Even though, one phase among the three phases will be presented.
- The generator is symmetrical.
- The generator is balanced in structure.
- The linearity of magnetization is considered.
- The stator is equipped by 3 phases voltage with the grid in a direct way.
- The rotor is equipped by 3 phases voltage but no related to the voltage of stator.
- We are representing one phase here, while the two other phases have the same exact model.

The following Figure 5.2 illustrates the equivalent circuit which models the steady state of a DFIGs system considering the aforementioned assumptions.

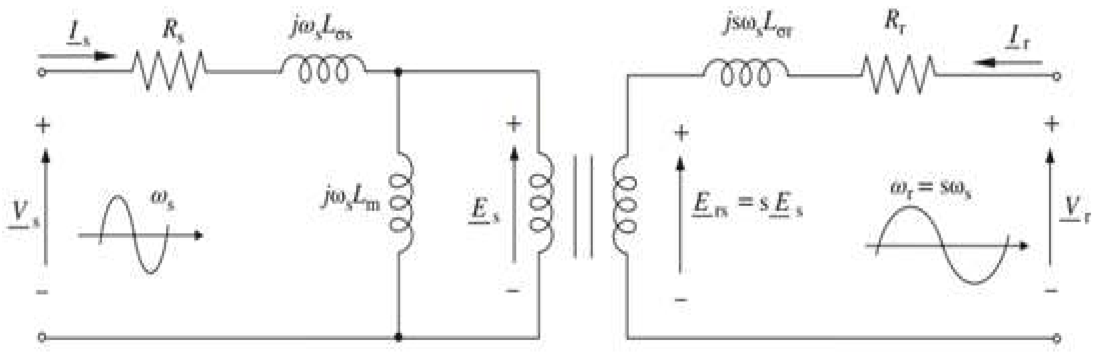

Figure 5.2 The equivalent circuit of the steady state (Abad et al. 2011)

In order to indicate the characterization of the previous circuit and determinate the steady state model, we have to define the electric parameters and magnitudes which are related to the rotor and stator as shown in the Figure 5.2.

We are defining here the coefficient μ which is equal to the ratio of the turns of stator N_S to the turns of the rotor N_R as Equation (5.4):

$$\mu = \frac{N_S}{N_R} \tag{5.4}$$

On the other hand, this coefficient represents the relation between the induced EMFs in the stator and rotor in terms of the slip s. This relation can be described in the following Equation (5.5):

$$\mu = \frac{N_S}{N_R} = s\frac{\overline{E_S}}{\overline{E_R}} \tag{5.5}$$

Where $\overline{E_S}$ is the magnitude of the stator's EMF and $\overline{E_R}$ is the magnitude of the rotor's EMF. We can observe that the two induced EMFs are equal when the turns of stator N_S are equal to the turns of the rotor $N_R$and the system is at steady state ($s = 1$).

In order to head toward the practical modeling, we prefer to describe the circuit in terms of one frequency instead of the both stator and rotor ones. In order to achieve that we choose to describe the circuit in terms of the stator frequency; therefore, the circuit related to the rotor has to be converted to the stator frequency as shown in the following Figure 5.3.

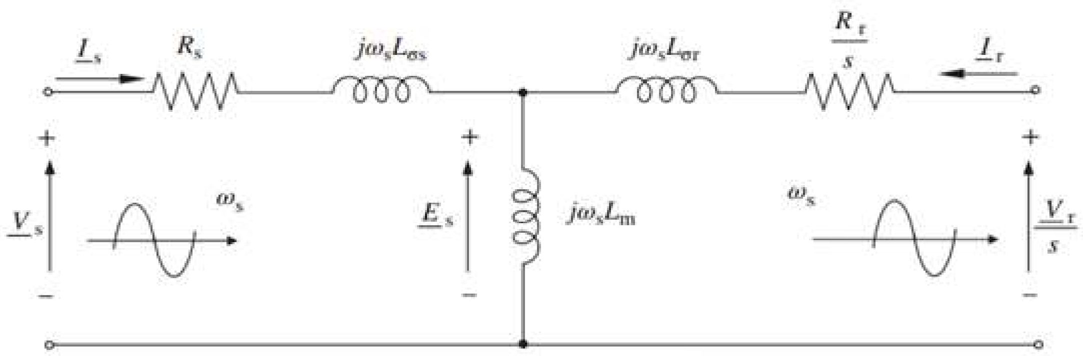

Figure 5.3 The equivalent circuit of the steady state (Abad et al. 2011)

According to the ultimate equivalent circuit Figure 5.3, we can write the electrical equations which dominate the steady state case for DFIGs are described in the following equation.

The electrical equations which are related to voltages are given as Equation (5.6) and Equation (5.7):

$$\frac{V_R}{s} = (\frac{R_R}{s} + j.\omega_S.L_R)\overline{I_R} + j.\omega_S.L_M.(\overline{I_R} + \overline{I_S}) \quad (5.6)$$

$$V_S = (R_S + j.\omega_S.L_S)\overline{I_S} + j.\omega_S.L_M.(\overline{I_R} + \overline{I_S}) \quad (5.7)$$

We can observe that the rotor frequency ω_R has been eliminated from the electrical equations. While the electrical equations which are related to fluxes are given Equation (5.8) and Equation (5.9):

$$\psi_R = L_M.(\overline{I_R} + \overline{I_S}) + L_R\overline{I_R} \quad (5.8)$$

$$\psi_S = L_M.(\overline{I_R} + \overline{I_S}) + L_S\overline{I_S} \quad (5.9)$$

Depending on the previous electrical equations, we can derive the phase diagram related to any operating case or working condition. We show an example for DFIG system operates at two different speeds. Figure 5.4 shows phase diagram related to two operating cases of slip.

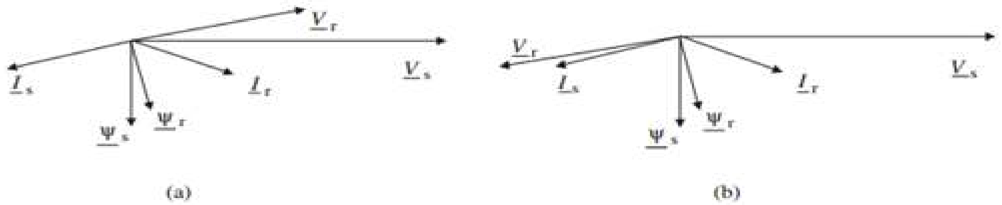

Figure 5.4 Phase diagram related to two operating cases of slip: a- s > 0 and b- s < 0 (Abad et al. 2011)

5.2.2 Power equations

The equality of power is caused by the balance of the power in the DFIG systems. The first side of this equality includes the active power of the rotor and the stator P_r, P_s respectively, while the other side refers to the mechanical power P_{mec} and in addition the losses in power P_{cu} which are caused by cupper in the stator and rotor. The balance of the power in the DFIG systems can be descried as in the following Equation (5.10) Equation (5.15)

$$P_{mec} - P_{cu} = P_R + P_S \tag{5.10}$$

$$P_{cu} = P_{cu,Stator} + P_{cu,Rotor} \tag{5.11}$$

$$P_{cu,stator} = 3 * R_S * |\overline{I_S}|^2 \tag{5.12}$$

$$P_{cu,rotor} = 3 * R_R * |\overline{I_R}|^2 \tag{5.13}$$

$$P_r = 3 * Real\ (\overline{V_R} * \overline{I_R}) \tag{5.14}$$

$$P_s = 3 * Real\ (\overline{V_s} * \overline{I_s}) \tag{5.15}$$

However, we can define the coefficient of efficiency γ which is related to the generator according to the value of the mechanical power P_{mec}. This coefficient γ is equal to the ratio of the mechanical power P_{mec} to the active power of the rotor and the stator P_r, P_s when P_{mec} is positive. As given Equation (5.16), while γ is equal to the ratio of the active power of the rotor and the stator P_r, P_s to the mechanical power P_{mec} when P_{mec} is negative.

$$\gamma = \begin{cases} \frac{P_{mec}}{P_R + P_s} & when\ P_{mec} > 0 \\ \frac{P_R + P_s}{P_{mec}} & when\ P_{mec} < 0 \end{cases} \tag{5.16}$$

In the same context, the reactive power is calculated using the following Equation (5.17) and Equation (5.18):

$$Q_R = 3 * Image(\overline{V_r} * \overline{I_r}) \tag{5.17}$$

$$Q_S = 3 * Image\ (\overline{V_s} * \overline{I_s}\ ) \tag{5.18}$$

Consequently, we can derive the equations of power by substituting the voltage formulas into the expressions of power as following Equation (5.19) Equation (5.23):

$$s = \frac{\omega_R}{\omega_S} \tag{5.19}$$

$$P_R = 3 * Real\ (\overline{V_R} * \overline{I_R}) = 3(-\omega_R . L_M . Image\ (\overline{I_s} * \overline{I_R})\ + R_r . |\overline{I_R}|^2) \tag{5.20}$$

$$P_s = 3 * Real\ (\overline{V_s} * \overline{I_s})\ = 3(\omega_S . L_M . Image\ (\overline{I_s} * \overline{I_R})\ + R_S . |\overline{I_S}|^2) \tag{5.21}$$

$$Q_R = 3 * Image(\overline{V_r} * \overline{I_r}) = 3(\omega_R . L_M . Real\ (\overline{I_s} * \overline{I_R}) + \omega_R . L_R . |\overline{I_R}|^2) \tag{5.22}$$

$$Q_S = 3 * Image\ (\overline{V_s} * \overline{I_s}\ ) = 3(\omega_S.L_M.Real\ (\overline{I_s} * \overline{I_R}) + \omega_S.L_S.|\overline{I_S}|^2) \tag{5.23}$$

5.2.3 Operation modes

We can express the developed electromagnetic torque in the shaft as Equation (5.24):

$$T_{em} = \frac{P_{mec}}{\Omega_M} = p * \frac{P_{mec}}{\Omega_R} \tag{5.24}$$

So, we can substitute the previous equations of power in this last formula of the developed electromagnetic torque in order to develop the torque as a function of the currents and parameters of machine as Equation (5.25):

$$T_{em} = 3 * p * L_M * Imag(\overline{I_s} * \overline{I_R}) \tag{5.25}$$

On the other hand, this last equation can be expressed as a function of the fluxes as shown in the following Equation (5.26):

$$T_{em} = \frac{3 * L_M}{\alpha * L_R * L_S} * Imag(\overline{I_s} * \overline{I_R}) \tag{5.26}$$

Where the factor α is expressed as Equation (5.27):

$$\alpha = 1 - \frac{{L_M}^2}{L_R * L_S} \tag{5.27}$$

Speaking of operation modes, it is possible to indicate four modes in DFIG as long as the four combinations of speed and torque are distinguished; the negative or positive torque and the hyper-synchronism and sub-synchronism speed (Grauers 1994). Figure 5.5 represents four modes in DFIG related to four combinations of speed and torque.

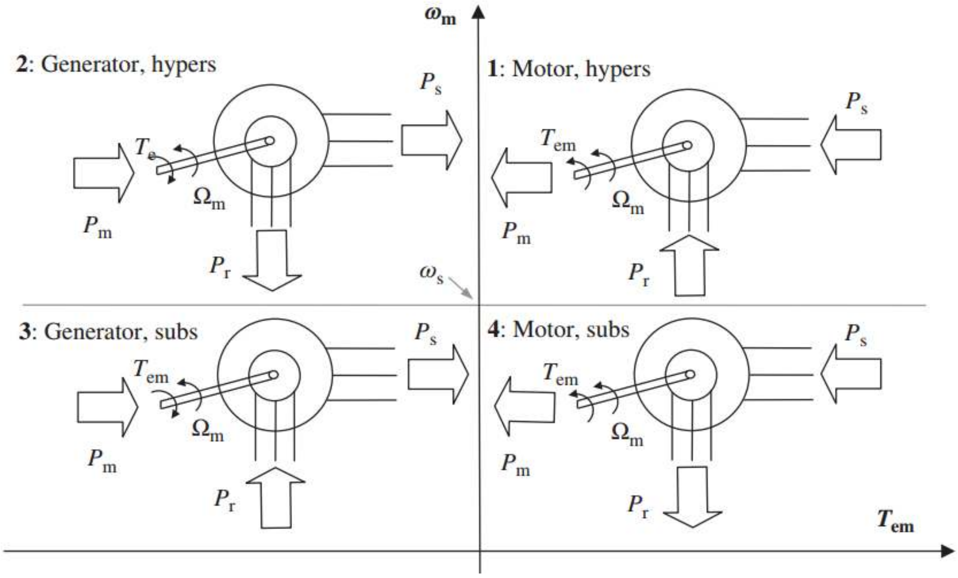

Figure 5.5 Four modes in DFIG related to four combinations of speed and torque (Abad et al. 2011)

We can observe that the hyper-synchronism is occurred when we have a negative slip and the active powers of rotor and stator provide the same sign.

5.2.4 Curves of torque

Considering the Thevenin circuit between the points X and Y, we can calculate the current of rotor and obtain the electromagnetic torque expression related to steady-state. However, we can obtain the mechanical power P_{mec} by computing the elements' power regarding the dependence of slip with the circuit.

The electromagnetic torque can be developed as a function of the current and voltage of rotor as Equation (5.28) and Equation (5.29):

$$T_{em} = \frac{3*p}{s*\omega_S} * \left(R_r * \overline{I_R}^2 - \overline{I_R} * \overline{V_R} * \cos\varphi\right) \tag{5.28}$$

$where$:

$$\varphi = ang\,(\overline{V_R} - \overline{I_R}) \tag{5.29}$$

The following Figure 5.6 shows the curves of torque regarding various rotor to stator voltage values. We can observe that when the voltage of rotor is zero, then we obtain ordinary curve of the squirrel-cage induction machine.

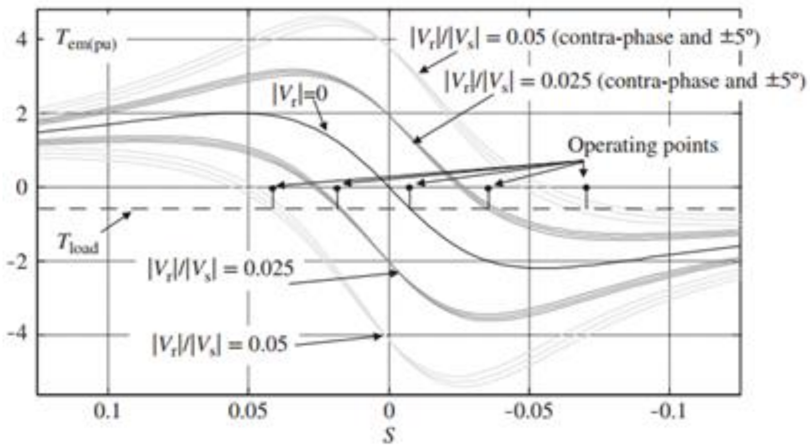

Figure 5.6 Curves of torque in terms of slip for various rotor to stator voltage values (Abad et al. 2011)

In addition, we can see that for the values 0.025 for rotor to stator voltage, the torque is equal to zero at two symmetric values of slips (i.e., ±0.025) and the phase ($\varphi = 0 \; or \; \pi$) between rotor and stator.

5.3 Dynamic Case

5.3.1 The model $\alpha\beta$

The theory related to space vector can be applied in order to develop the dynamic $\alpha\beta$ model considering the linearity and ideal conditions. The following figure illustrates the various reference rotating frames which are adopted typically in order to develop DFIG space vector models. The reference frame of stator is stable, while the (DQ) reference frame of rotor rotates at the speed Ω_M and the (dq) synchronous frame rotates at the speed ω_S. Adopting the inverse and direct transformation, the space vector is represented using DQ, dq or $\alpha\beta$ frame and various references frames related to DFIG space vectors are represented in Figure 5.7.

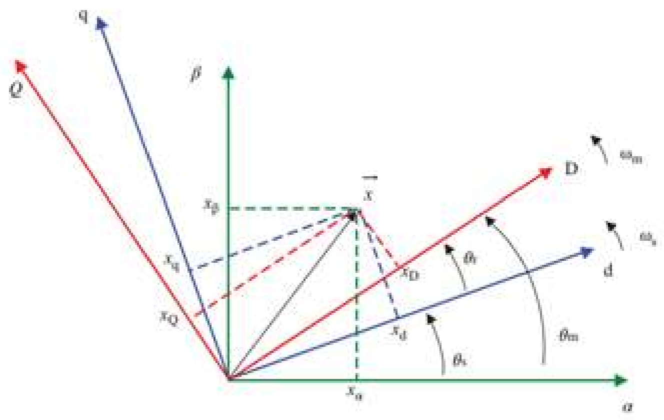

Figure 5.7 Various references frames related to DFIG space vectors (Abad et al. 2011)

Consequently, the rotor and stator voltages can be expressed or transformed to the stationary voltages related to $\alpha\beta$ frame as follows, we have to point to those voltages and currents of rotor are relative to the stator.

For the rotor voltages Equation (5.30) can be used, as:

$$V_R = R_R \overline{I_R} + \frac{d\psi_R}{dt} - j * \Omega_M * \psi_R \tag{5.30}$$

Transforming to the stationary voltages related to $\alpha\beta$ frame given as Equation (5.31):

$$\begin{aligned} V_{\alpha R} &= R_R \overline{I_{\alpha R}} + \frac{d\psi_{\alpha R}}{dt} + \Omega_M * \psi_{\beta R} \\ V_{\beta R} &= R_R \overline{I_{\beta R}} + \frac{d\psi_{\beta R}}{dt} - \Omega_M * \psi_{\alpha R} \end{aligned} \tag{5.31}$$

For the stator voltages Equation (5.32) can be used, as:

$$V_S = R_S \overline{I_S} + \frac{d\psi_S}{dt} \tag{5.32}$$

Transforming to the stationary voltages related to $\alpha\beta$ frame given as Equation (5.33):

$$V_{\alpha S} = R_S\overline{I_{\alpha S}} + \frac{d\psi_{\alpha S}}{dt}$$
$$V_{\beta S} = R_S\overline{I_{\beta S}} + \frac{d\psi_{\beta S}}{dt} \quad (5.33)$$

Similarly, the fluxes related to rotor and stator can be expressed or transformed to the stationary voltages related to $\alpha\beta$ frame as given as Equation (5.34) Equation (5.37).

For the rotor fluxes:

$$\psi_R = L_M.\overline{I_S} + L_R\overline{I_R} \quad (5.34)$$

Transforming to the stationary voltages related to $\alpha\beta$ frame gives us:

$$\psi_{\alpha R} = L_M.\overline{I_{\alpha R}} + L_R\overline{I_{\alpha R}}$$
$$\psi_{\beta R} = L_M.\overline{I_{\beta S}} + L_R\overline{I_{\beta S}} \quad (5.35)$$

For the stator fluxes:

$$\psi_S = L_S.\overline{I_S} + L_M\overline{I_R} \quad (5.36)$$

Transforming to the stationary voltages related to $\alpha\beta$ frame gives us:

$$\psi_{\alpha S} = L_M.\overline{I_{\alpha S}} + L_S\overline{I_{\alpha R}}$$
$$\psi_{\beta S} = L_M.\overline{I_{\beta S}} + L_S\overline{I_{\beta S}} \quad (5.37)$$

So, the equivalent circuit shown in the Figure 5.8 is corresponding to DFIG model in the $\alpha\beta$ reference frame. We can note that all currents, fluxes and voltages are sinusoid signals in term of ω_S frequency.

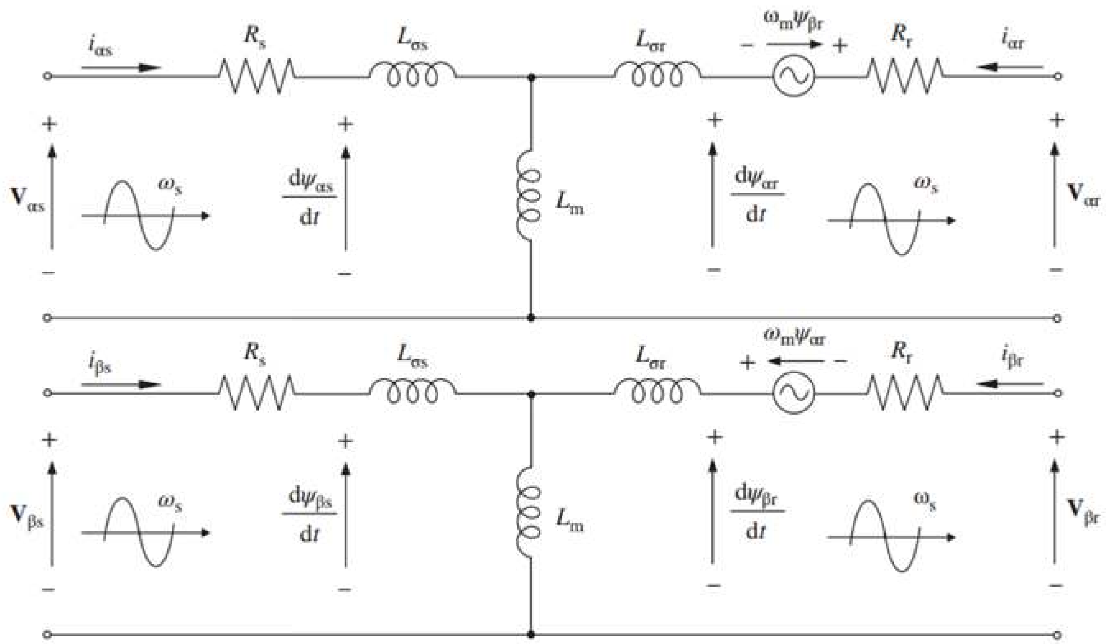

Figure 5.8 $\alpha\beta$ reference frame of the DFIG model (Abad et al. 2011)

In addition, the powers related to rotor and stator can be expressed in $\alpha\beta$ reference frame as between Equation (5.38) and Equation (5.41):

$$P_R = \frac{3}{2} * (V_{\alpha R} * I_{\alpha R} + V_{\beta R} * I_{\beta R}) \tag{5.38}$$

$$P_s = \frac{3}{2} * (V_{\alpha S} * I_{\alpha S} + V_{\beta S} * I_{\beta S}) \tag{5.39}$$

$$Q_R = \frac{3}{2} * (-V_{\alpha R} * I_{\beta R} + V_{\beta R} * I_{\alpha R}) \tag{5.40}$$

$$Q_S = \frac{3}{2} * (-V_{\alpha S} * I_{\beta S} + V_{\beta S} * I_{\alpha S}) \tag{5.41}$$

The electromagnetic torque can be developed as a function of the current and voltage of rotor as Equation (5.42):

$$T_{em} = \frac{3}{2} * p\left(\psi_{\beta R} * I_{\alpha R} - \psi_{\alpha R} * I_{\beta R}\right) \tag{5.42}$$

5.3.2 The model dq

The theory related to space vector can be applied in order to develop the synchronous dq model of DFIG considering the linearity and ideal conditions. In order to obtain the rotor and stator voltages as expressed or transformed to dq synchronous frame, we can multiply the equations by $e^{-j\theta_S}$ and $e^{-j\theta_R}$ as follows; we have to point to those voltages and currents of rotor are relative to the stator.

For the rotor voltages Equation (5.43) can be used, as:

$$V_R = R_R\overline{I_R} + \frac{d\psi_R}{dt} + j * \Omega_M * \psi_R \tag{5.43}$$

Transforming to the stationary voltages related to dq frame given as Equation (5.44):

$$\begin{aligned} V_{dR} &= R_R\overline{I_{dR}} + \frac{d\psi_{dR}}{dt} - \omega_R * \psi_{qR} \\ V_{qR} &= R_R\overline{I_{qR}} + \frac{d\psi_{qR}}{dt} + \omega_R * \psi_{qR} \end{aligned} \tag{5.44}$$

For the stotor voltages Equation (5.45) can be used, as:

$$V_S = R_S\overline{I_S} + \frac{d\psi_S}{dt} \tag{5.45}$$

Transforming to the stationary voltages related to dq frame given as Equation (5.46):

$$\begin{aligned} V_{dS} &= R_S\overline{I_{dS}} + \frac{d\psi_{dS}}{dt} \\ V_{qS} &= R_S\overline{I_{qS}} + \frac{d\psi_{qS}}{dt} \end{aligned} \tag{5.46}$$

Similarly, the fluxes related to rotor and stator can be expressed or transformed to the stationary voltages related to dq frame as given as Equation (5.47) Equation (5.50).

For the rotor fluxes:

$$\psi_R = L_M.\overline{I_S} + L_R\overline{I_R} \tag{5.47}$$

Transforming to the stationary voltages related to $\alpha\beta$ frame gives us:

$$\begin{aligned} \psi_{dR} &= L_M.\overline{I_{dR}} + L_R\overline{I_{dR}} \\ \psi_{qR} &= L_M.\overline{I_{qS}} + L_R\overline{I_{qS}} \end{aligned} \tag{5.48}$$

For the stator fluxes:

$$\psi_S = L_S.\overline{I_S} + L_M\overline{I_R} \tag{5.49}$$

Transforming to the stationary voltages related to dq frame gives us:

$$\begin{aligned} \psi_{dS} &= L_M.\overline{I_{dS}} + L_S\overline{I_{dR}} \\ \psi_{qS} &= L_M.\overline{I_{qS}} + L_S\overline{I_{qS}} \end{aligned} \tag{5.50}$$

So, the equivalent circuit shown in the Figure 5.9 is corresponding to DFIG model in the dq reference frame. We can note that all currents, fluxes and voltages are sinusoid signals in term of ω_S frequency.

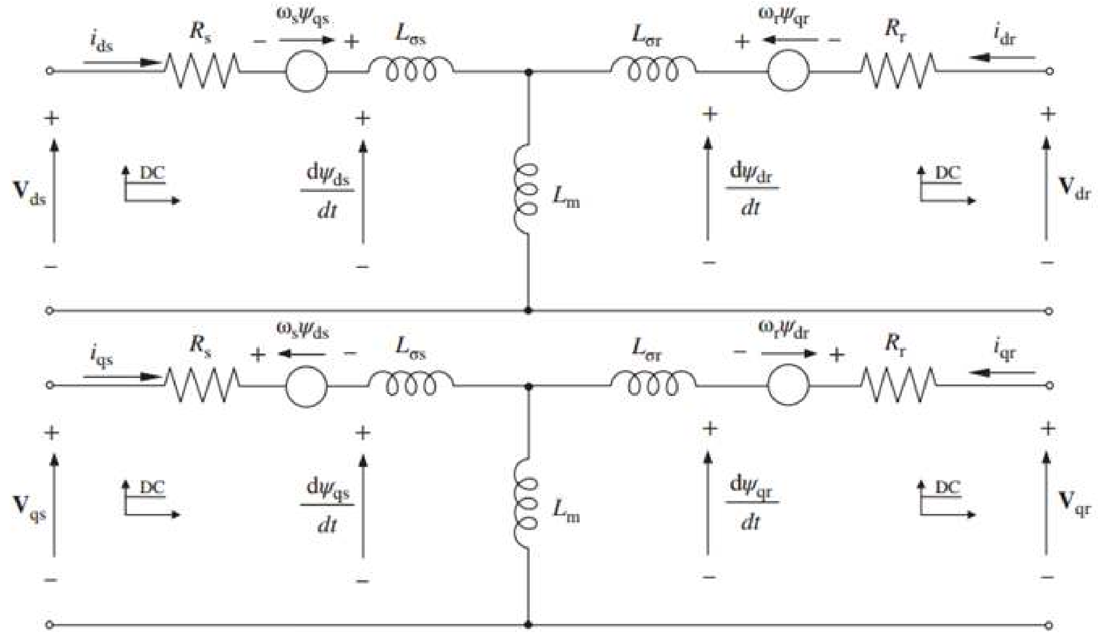

Figure 5.9 dq reference frame of the DFIG model (Abad et al. 2011)

5.4 Vector Control of DFIG

Related to the control of DFIG, we have to consider two main scenarios; (i) the Operating scenario in Grid Connection. (ii) The stand-alone Operating scenario. These two scenarios differ significantly from each other. In this section, we are presenting the control process related to the rotor side.

5.4.1 Current control loops

Among all the various techniques which are adopted in controlling DFIG, the vector control method is considered as the most effective and adopted over other ones. In the following titles, we simplify this method by discussing the control loops of current, developing steady state control.

The vector control technique is applied in a synchronous rotating frame as shown in following Figure 5.10, considering the aligned d-axis with the vector of stator flux (Abad et al. 2011) and (Pena et al. 1996).

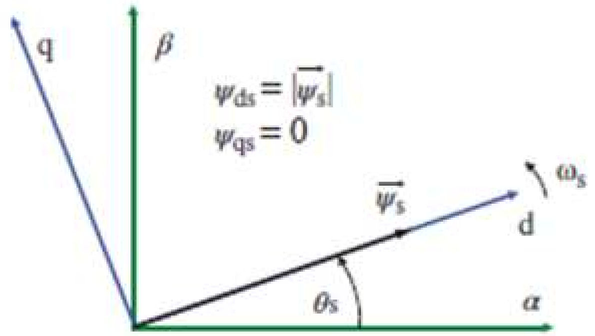

Figure 5.10 Synchronous rotating dq frame where d-axis aligned with the vector of stator flux (Abad et al. 2011)

Considering the DFIG model in a synchronous and reference frame, we can derive the voltage of rotor equations as given Equation (5.51) in terms of currents of rotor and flux of stator regarding that the q component of stator flux is equal to zero (ψ_{qS}).

$$V_{dR} = R_R I_{dR} + \sigma\, L_R \frac{dI_{dR}}{dt} - \omega_R\, \sigma\, L_R\, I_{qR} + \frac{L_M}{L_S} \frac{d\overline{\psi_S}}{dt}$$
$$V_{qR} = R_R I_{qR} + \sigma\, L_R \frac{dI_{qR}}{dt} - \omega_R\, \sigma\, L_R\, I_{dR} + \omega_R \frac{L_M}{L_S}\, \overline{\psi_S} \qquad (5.51)$$

Considering the two last equations, we can observe that if any small drop in stator has been occurred, then the flux of stator is stable and the term $\frac{d\overline{\psi_S}}{dt}$ is equal to zero, due to the direct connection between stator and grid at stable AC voltage. In addition, performing dq control for the rotor current is possible considering these two equations and adopting a regulator for every component of current as illustrated in the Figure (5.11). We can notice that the stator flux $\psi_S$and the velocity ω_R and the angle θ_R have to be estimated. Furthermore, the control process has to be applied in the dq space frame regarding that the currents and voltages of the rotor have to be converted to DQ coordinates. In order to obtain θ_S, the angle of the voltage vector of rotor is computed or estimated and then subtract 90 degrees from it. In addition, the synchronization of the stator voltage grid is established using any phase locked loop (PLL) which guarantees robust estimation and absence of harmonics. Eventually, we have to point to that the loops of control in the Figure 5.11 are applied regarding those currents of rotor are relative to the stator.

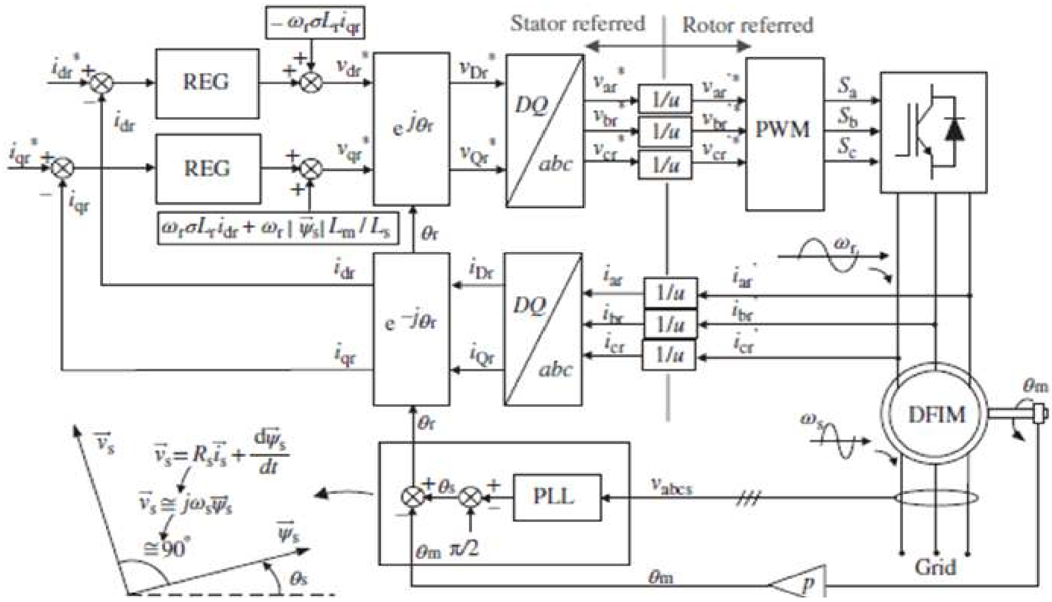

Figure 5.11 Loops of current control in DFIG (Abad et al. 2011)

The following Figure 5.12 illustrates that adopting the same PI regulator for each loop and regardless the impact of converter of the voltage source and delays related to measuring and computing operations, the closed loops which are equivalent to current loops are considered as a system of 2nd order and with zero and two poles.

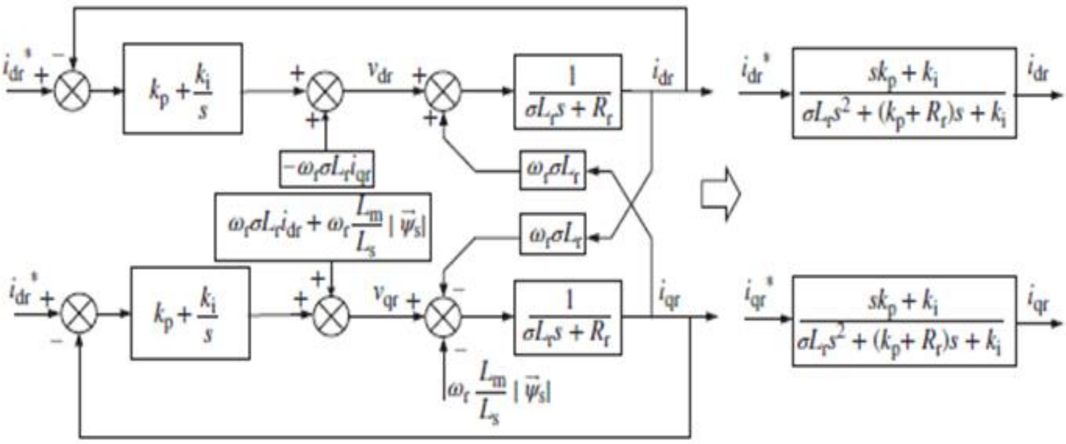

Figure 5.12 Equivalent system of 2nd order for loop of the current control (Abad et al. 2011)

5.4.2 Speed and power control loops

In the light of the previous study of the control loops of current, the overall control loops (Speed and power control) can be presented. Considering the aligned d-axis with the vector of stator flux, the electromagnetic torque can be developed as a function of the q component of rotor current as Equation (5.52) and Equation (5.53):

$$T_{em} = \frac{3}{2} * p\left(\psi_{\beta R} * I_{\alpha R} - \psi_{\alpha R} * I_{\beta R}\right) = \frac{3}{2} * p * \frac{L_M}{L_S}\left(\psi_{qS} * I_{dR} - \psi_{dS} * I_{qR}\right) \tag{5.52}$$

$$T_{em} = \frac{3}{2} * p * \frac{L_M}{L_S} \overline{\psi_S}\, I_{qR} \tag{5.53}$$

We can observe that the q component of rotor current is directly proportional to resultant electromagnetic torque and the machine's speed. Similarly for the reactive power of the stator expressed in the dq frame, we can write as Equation (5.54) and Equation (5.55):

$$Q_S = \frac{3}{2} * \left(-V_{qS} * I_{dS} - V_{dS} * I_{qS}\right) \tag{5.54}$$

$$Q_S = \frac{3}{2} * \frac{L_M}{L_S} * \omega_S * \overline{\psi_S}\left(I_{dR} - \frac{\overline{\psi_S}}{L_M}\right) \tag{5.55}$$

We can observe that the d component of rotor current is directly responsible for the reactive power of the stator Q_S.

Taking into account the adopted orientation, the components of the rotor's current guarantee the possibility to control the reactive power of the stator beside the torque. Considering the equations and expressions which are derived in this section, the Figure 5.13 shows the overall control loops related to the DFIG. We can notice the addition of the loop related to the reactive power of the stator Q_S and the loop of speed.

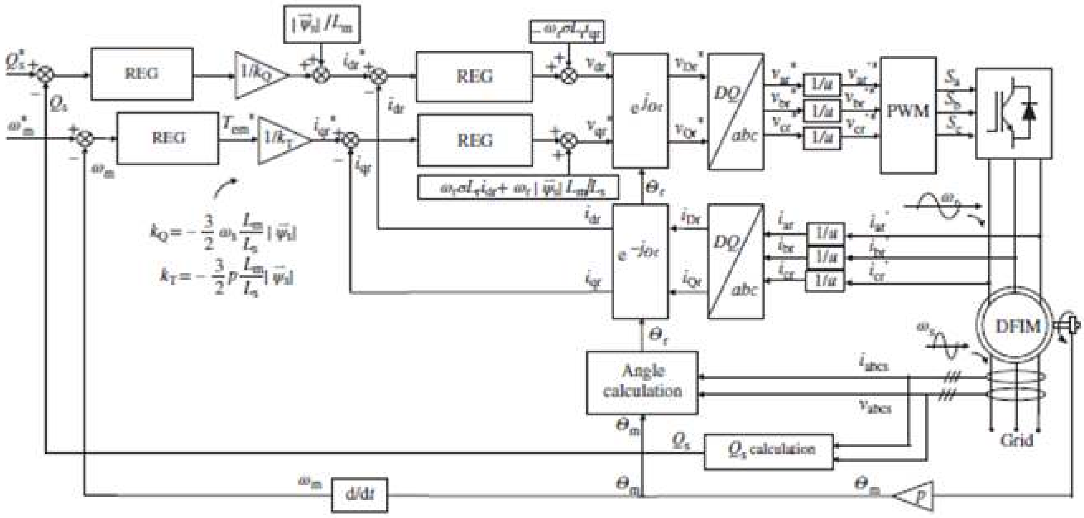

Figure 5.13 Overall control loops related to the DFIG (Abad et al. 2011)

As mentioned before, the flux's amplitude of the stator is constant due to the direct connection between the grid and stator. The formula of this flux's amplitude can be expressed in term of the stator voltage as Equation (5.56):

$$\overline{\psi_S} \sim \frac{\overline{V_S}}{\omega_S} \quad (5.56)$$

therefore, the dq components of the flux's amplitude of the stator can be derived in the following relations as Equation (5.57) and Equation (5.58):

$$\psi_{dS} = L_S * I_{dS} + L_M * I_{dR} \quad (5.57)$$

$$\psi_{qS} = L_S * I_{qS} + L_M * I_{qR} \quad (5.58)$$

We can observe that indicating the I_{dS} and I_{dR} creates the level of the flux which in turn indicate the current amount between the stator side and the rotor one. On the other hand, the torque indicates the values of I_{qS} and I_{qR} which means that it is not possible to indicate or choose.

However, the following Figure 5.14 illustrates that adopting the same PI regulator for each loop and regardless the impact of converter of the voltage source and delays related to measuring and computing operations, the closed loops which are equivalent to current loops are considered as a system of 2nd order and with zero and two poles.

Recalling the control loops of current which are done before, the following Figure 5.14 illustrates the closed loop and equivalent system of the reactive power of stator Q_S and angular speed of machine ω_S which assumes that loops of current are tuned fast relative to the external loop regardless the impact of converter variation and delays related to measuring and computing operations.

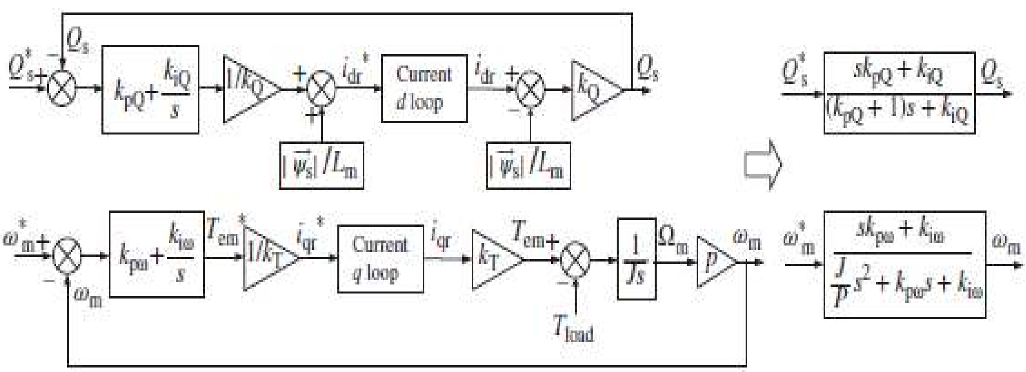

Figure 5.14 Closed loop and equivalent system of the reactive power of stator $\boldsymbol{Q_S}$ and angular speed of machine $\boldsymbol{\omega_S}$ (Abad et al. 2011)

5.5 Symmetrical Voltage Dips

The sudden drop in the voltage of the grid is known as a voltage dip. This drop may be caused by any error in the network. We are analyzing here a case of dealing with a Symmetrical Voltage Dips, also the behavior of the system will be addressed regarding the impact on the stator flux. In order to understand the voltage dips, the following interesting formula is derived as Equation (5.59):

$$\frac{d\psi_S}{dt} = V_s - \frac{R_S}{L_S} * \psi_S + R_S * \frac{L_M}{L_S} * I_R \qquad (5.59)$$

We can observe that when the voltage dip takes a place, the flux of stator can't reach its stable value in the steady state as fast as its voltage. Besides, the rotor current may contribute in make the decay of the flux faster as shown in the following Figure 5.15. It worth to point to that when the control is lost, the converter of the rotor side is responsible for controlling the current of rotor.

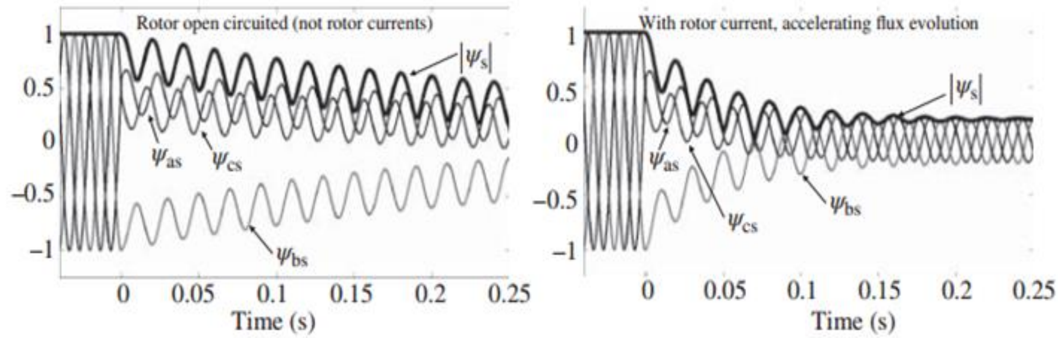

Figure 5.15 Rotor current impact on flux of stator evolution (Abad et al. 2011)

However, it will be useful to describe the equivalent circuit as shown in the Figure 5.16 to evaluate the voltage dips case. This equivalent circuit leads to write the following expression as Equation (5.60), which expresses the rotor voltage in term of the rotor and stator voltage, the equivalent inductances and resistances and the flux of stator:

$$V_R = \left(\left[\frac{L_M}{L_S}\right]^2 * R_S + R_R\right) * I_R + \frac{L_M}{L_S}\left(V_S - j * \omega_M * \psi_S\right) + \sigma * L_R * \frac{d}{dt} I_R \tag{5.60}$$

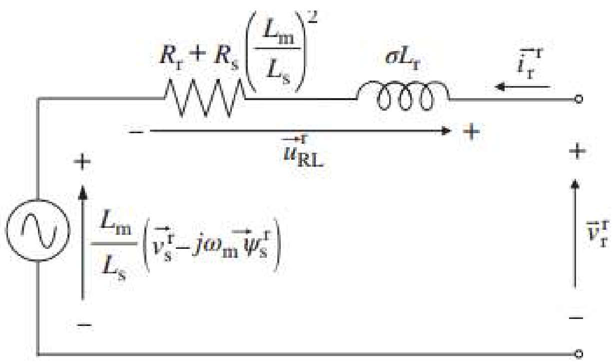

Figure 5.16 Equivalent circuit for voltage dips case (Winkelaar 1991)

Therefore, when the sudden drop in voltage occurs while the machine is operating at the steady state, the sudden change in the voltage of the stator should be addressed with a sudden change in the voltage of the rotor in order to protect the machine from any high value in the current of the rotor. We can observe that a higher value of rotor voltage is required, comparing to its values in the steady state, as a result of the decrease in the flux of stator in a slow manner (several number of cycles according to the machine characterizes) as shown in the Figure 5.17.

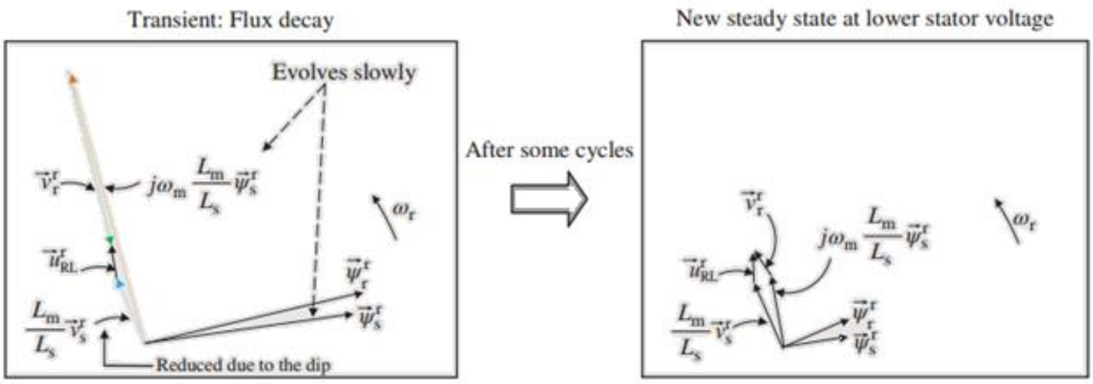

Figure 5.17 Evaluation of voltage dips case (Abad et al. 2011)

When these cycles are done, a new steady or stable state is reached but a decrease in the amplitudes are delivred which in turns caused a decrease in the reactive power of stator Q_S and the electromagnetic torque T_{em}. In order to deal with this case, a protection for the system is required which guarantee recovering the control after as less as possible of cycles. This may be done by adopting a crowbar protection as shown in the following Figure 5.18.

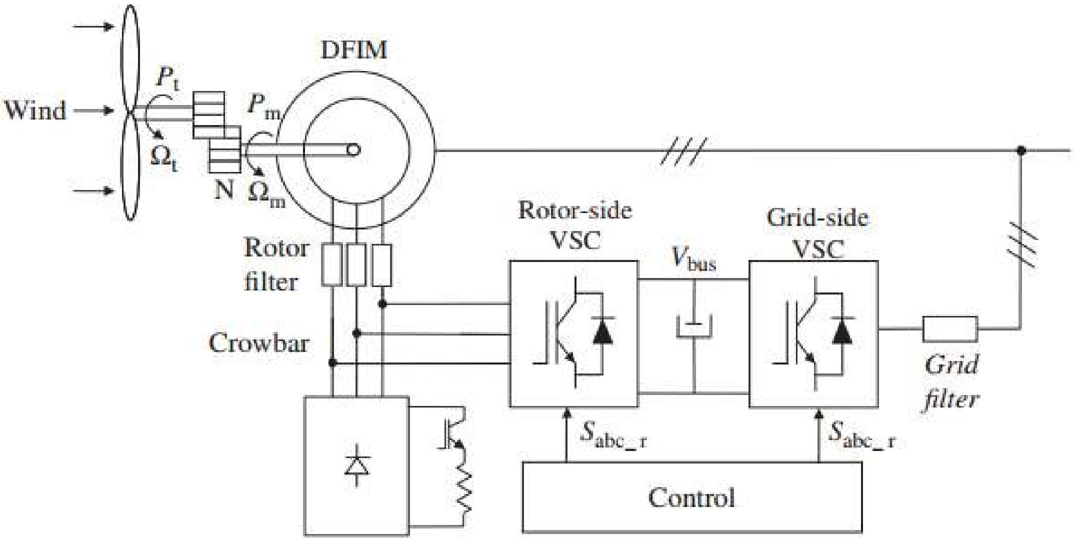

Figure 5.18 Crowbar protection in voltage dips case (Abad et al. 2011)

The following Figure 5.19 shows the equivalent circuit related to one phase of the DFIG system while the crowbar protection is achieved.

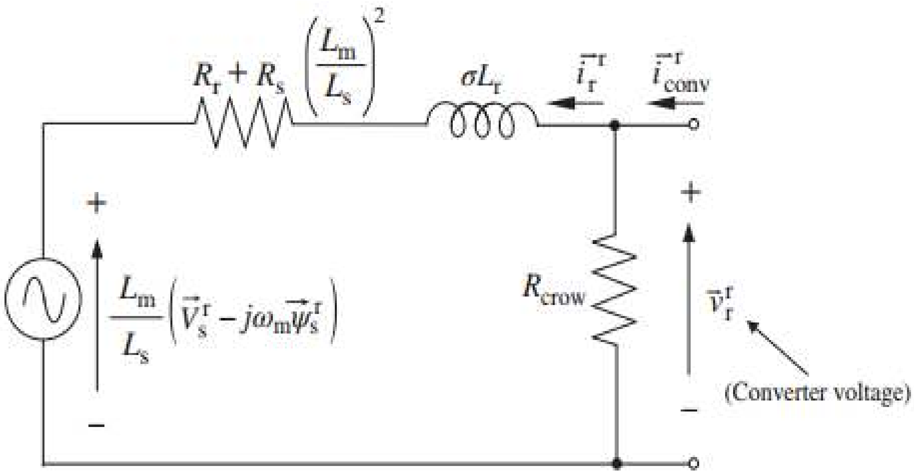

Figure 5.19 The equivalent circuit related to one phase of the DFIG system (Abad et al. 2011)

6. MODELING OF DFIG CONTROL

In this section, we are about to implement and model the previous theoretical concepts of controlling DFIG systems. The implementation process will go through sequential steps and subsystems in order to implement the complete controlling systems while various issues will be evaluated and discussed through the modulation process. Furthermore, the implementation and modulation process will be carried out based on MATLAB/ Simulink environment. The sequential stages of the modulation process are as follows:

- Implementation of the DFIG System (Control loops of rotor current, DFIG connection).
- Evaluation of Steady State Case.
- Implementation of Wind Turbine Model.
- Modeling and Connection of Back-to-Back Converter.
- Implementation of the overall DFIG System (Control loops of rotor and grid sides, DFIG connection, Wind Turbine Model).
- Evaluation of Symmetrical Voltage Dips.
- Evaluation of Dynamic Case.

6.1 Implementation of the DFIG System

The Wind Turbine System based on Doubly Fed Induction Generator (DFIGs) which is equivalent to constant frequency generator, this method is illustrated in the following Figure 6.1.

In this very step, we are modeling as an initial model the part in the red color which includes the control loops of rotor current and DFIG connection.

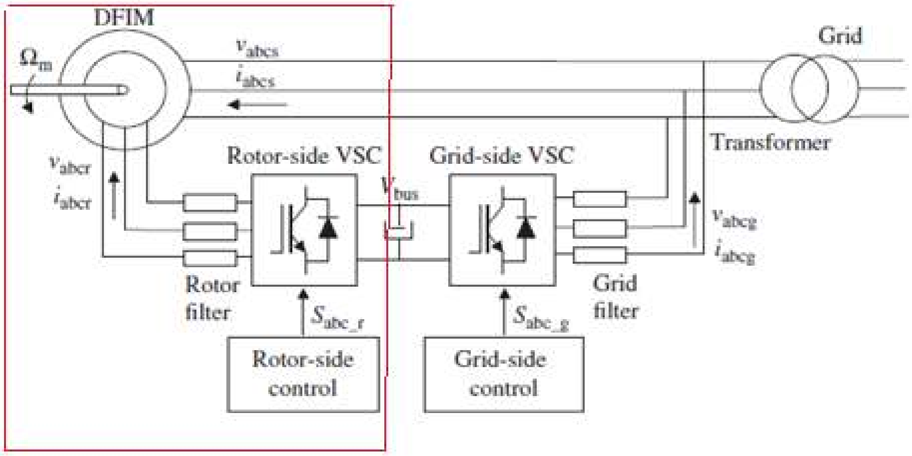

Figure 6.1 Initial model of DFIG system (Abad et al. 2011)

As shown in the following Figure 6.2, this initial system consists basically of the following main blocks:

- Three Phase Programmable Voltage Source.
- An Asynchronous Machine.
- Universal Bridge.
- Rotor Side Control Subsystem.

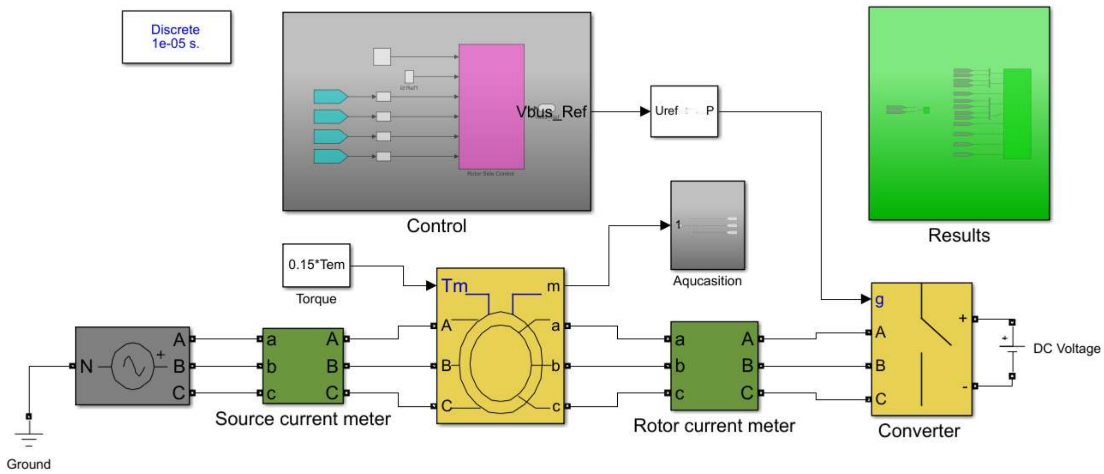

Figure 6.2 Initial system in MATLAB/ Simulink environment

We are presenting here, in this initial model, the input torque for the asynchronous machine as a constant value while in the upcoming modeling it will be the resultant torque which comes from the wind turbine model. As shown in the following Figure 6.3, the acquisition block includes the output parameters (Rotor Angle Theta, Rotor Speed and Electromagnetic Torque) of the asynchronous machine which matter us and used in the Rotor Side Control Subsystem.

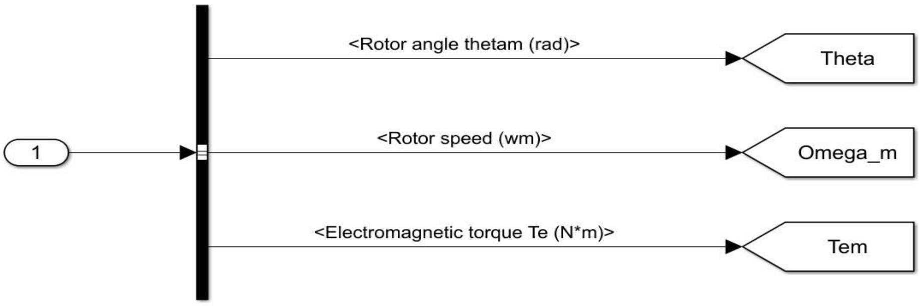

Figure 6.3 Acquisition block in the DFIG model

The block where the control method is implemented is the Rotor Side Control Subsystem as shown in the following Figure 6.4. This block takes as an input the parameters;(rotor speed, reference speed, estimated value of rotor current, rotor angle theta and source voltage) while the output is the voltage of Bus which is the input of the PWM generator. Eventually, we have to point to that the loops of control in the Figure 6.4 are applied regarding those currents of rotor are relative to the stator.

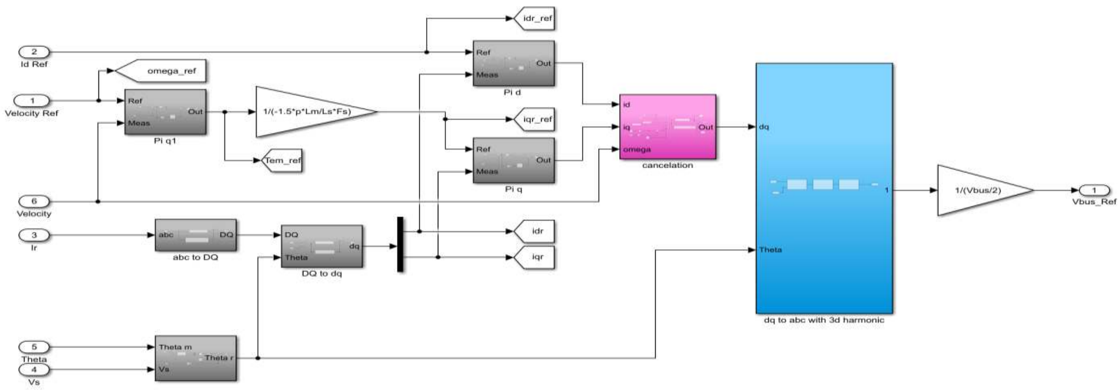

Figure 6.4 Rotor side control subsystem

This subsystem is the implementation of the Current Control Loop which is discussed before and illustrated in the Figure 6.4. Furthermore, we have to point here that all the values related to machine's parameters, PI regulator and references and correction values are set and adjusted in a MATLAB code file and linked to the Simulink model. The results related to the evaluation and run of this model in this stage are discussed and shown in the following figures.

The three phases programmable voltage source is responsible for an input of 690 Volt Vrms and 50Hz frequency as shown in the following Figure 6.5.

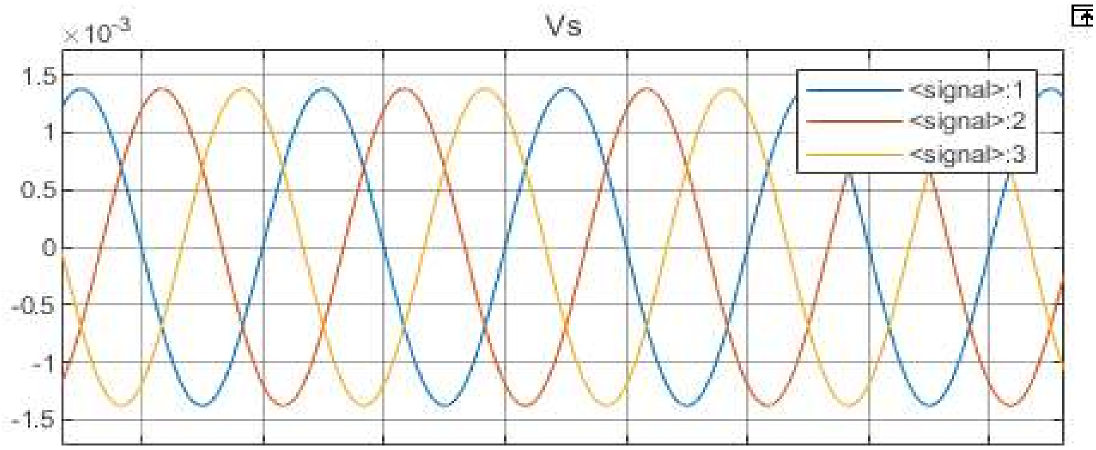

Figure 6.5 Signal of three phases programmable voltage source

The reference or objective speed is entered as a step signal with an initial value of 140 m/sec and 157 m/sec as a final value as shown in the following Figure 6.6. According to the machine adopted, we computed the synchronous speed as 157 m/sec. In addition, we are presenting the torque signal.

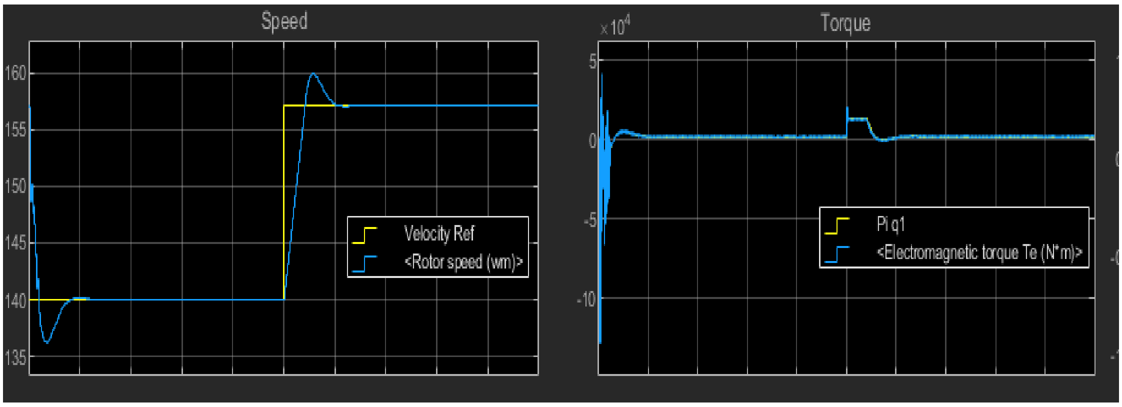

Figure 6.6 Reference and controlled speed

We can observe that the control process is done with 0.15-time response and 2.5% override and zero final error. The control loop is responsible for chasing the reference or objective speed even with the change in the value. On the other hand, the control process of the current is done as shown in the following Figure 6.7, while the method of zero value of the d component related to the rotor current is adopted.

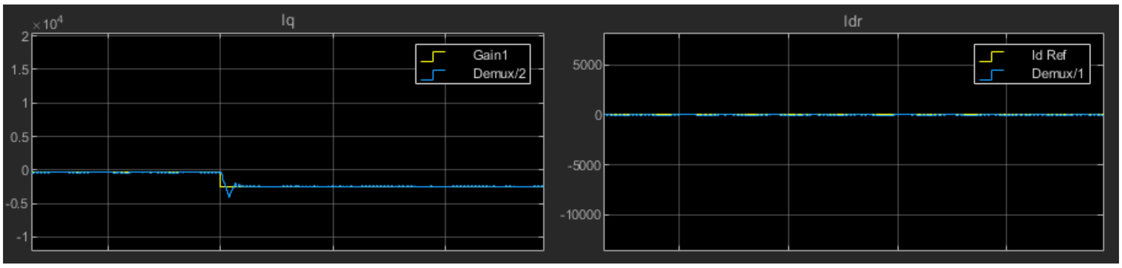

Figure 6.7 Control process of the current

In addition, we are presenting the current of the rotor and stator according to the input step of the objective speed as illustrated in the following Figure 6.8. Referring to the transition phase, we note that an increase in the current of stator is exerted until it returns to its stable phase as long as the speed is constant.

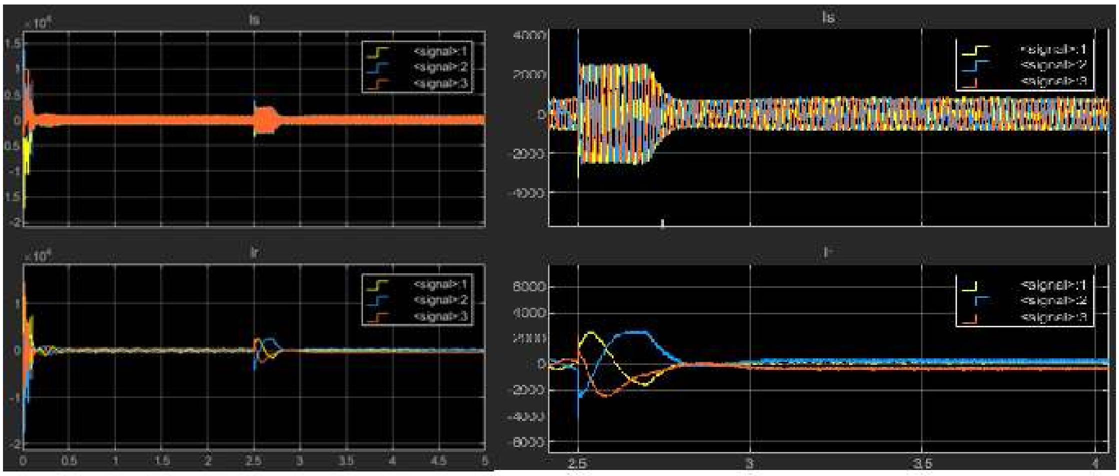

Figure 6.8 Current of the rotor and stator according to the input step of the objective speed

We can observe in the transition phase and for the rotor current that at the synchronous speed, the current of rotor is developed a DC current which point to the synchronization phase in DFIG system.

Eventually, we are presenting the d and q components of rotor voltage according to the input step of the objective speed as illustrated in the following Figure 6.9. Referring to the transition phase, we note that the average value of the d components of rotor voltage is zero while the average value of q components of rotor voltage is about 50 volts for the initial speed and zero at the synchronous speed.

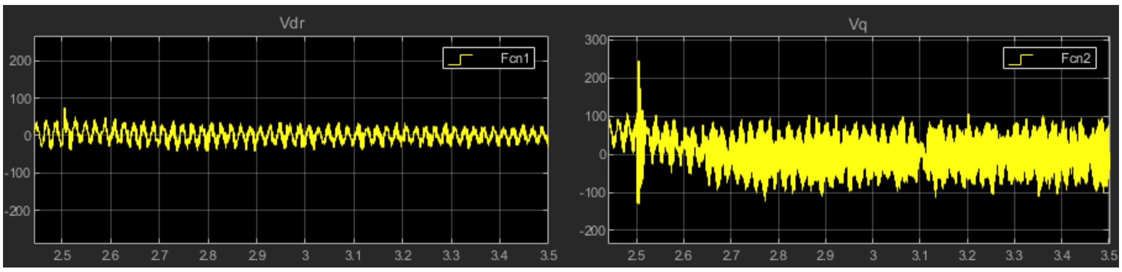

Figure 6.9 The d and q components of rotor voltage according to the input step of the objective speed

It worth to mention that we are neglecting the initial response at the beginning moment, because we are considering that the rotor and stator is connected permanently, while it is not the case in the real implementation. Therefore, a pick in all signals is exerted at the beginning moment as shown in the following Figure 6.10 as an example.

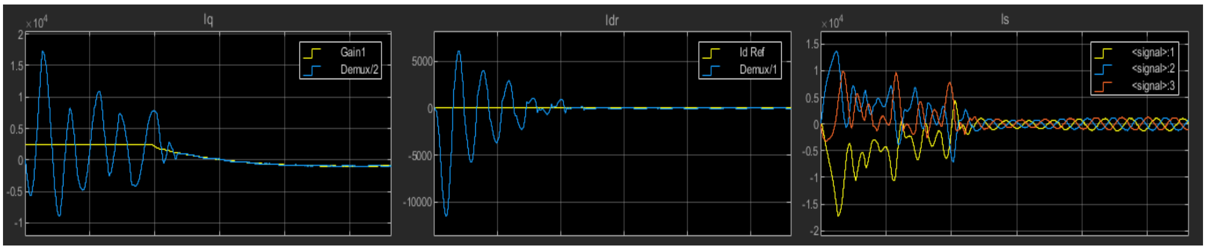

Figure 6.10 Evaluation of initial response at the beginning moment

6.2 Steady State Behavior

Considering the analysis of the steady state behavior related to the DFIG which is discussed before and the operation of wind turbine in the previous sections, it is possible to evaluate and implement the control loops and equations related to the steady state case. This behavior or performance can be derived at either the stator flux is zero or the d component of the rotor current is zero. These two methods will be shown in the following figures regarding that the electromagnetic torque and mechanical power are the input of the DFIG shaft and observing that the produced values of the mechanical power and electromagnetic torque is higher at higher values of the speed regarding the slips are at minimum.

In order to evaluate and implement the steady state in our model, we consider the value of the rotational speed as n = 1365 rpm as shown in the following Figure 6.11. In addition, this value will be considered as the objective point in the theorical performance figures.

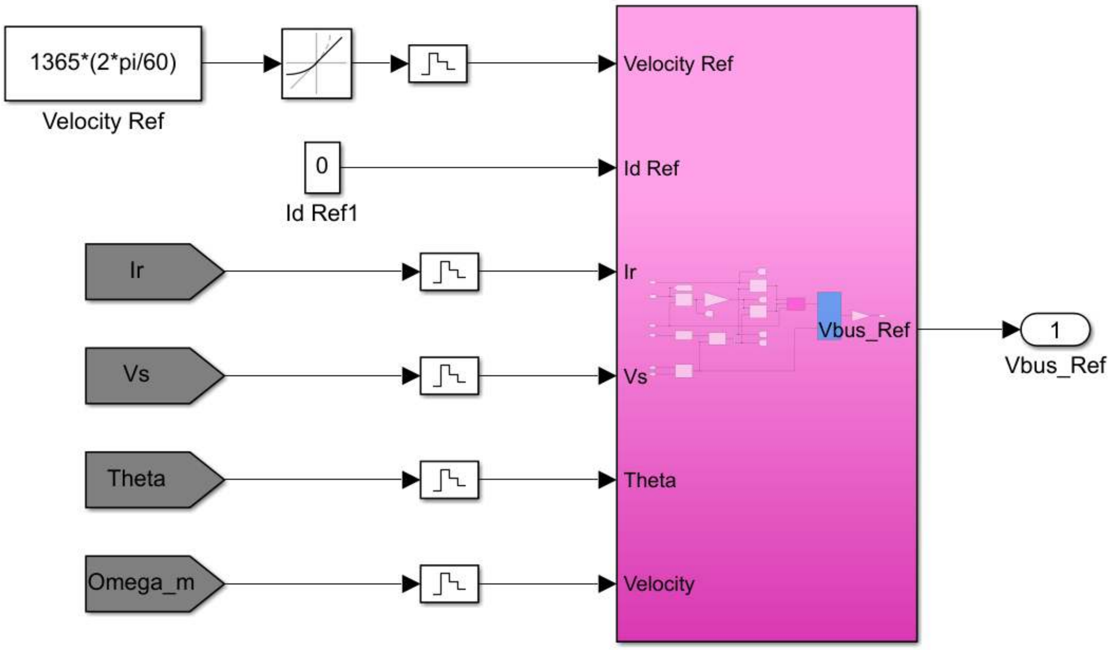

Figure 6.11 Value of the rotational speed as n = 1365 rpm

In the following figures, the steady state behavior in red color refers to the stator flux is zero $Q_S = 0$, while in blue color refers to the d component of the rotor current is zero.

The following Figure 6.12 shows the electromagnetic torque and mechanical power and the power of the stator and rotor. Note that the two methods are exact the same as long as these parameters are the input of the DFIG system. However, the corresponding values of these parameters at the rotational speed n = 1365 rpm are taken into account.

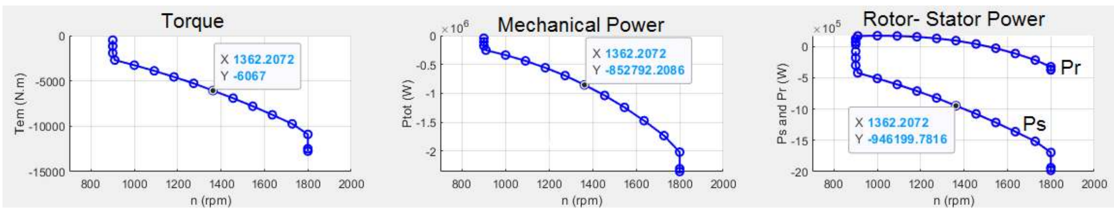

Figure 6.12 Electromagnetic torque and mechanical power and the power of the stator and rotor

In addition, the following Figure 6.13 shows the current and voltage related to the rotor and stator in the steady state behavior (in red $Q_S = 0$ while in blue $I_{dr} = 0$). However, the corresponding values of these parameters at the rotational speed n = 1365 rpm are taken into account.

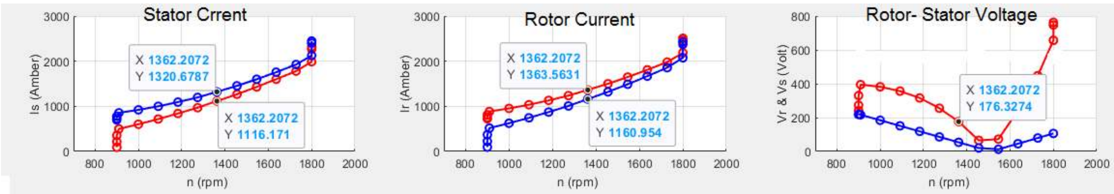

Figure 6.13 Current and voltage related to the rotor and stator in the steady state behavior

Finally, the following Figure 6.14 shows the flux related to the rotor and stator and the efficiency in the steady state behavior (in red $Q_S = 0$ while in blue $I_{dr} = 0$). However, the corresponding values of these parameters at the rotational speed n = 1365 rpm are taken into account.

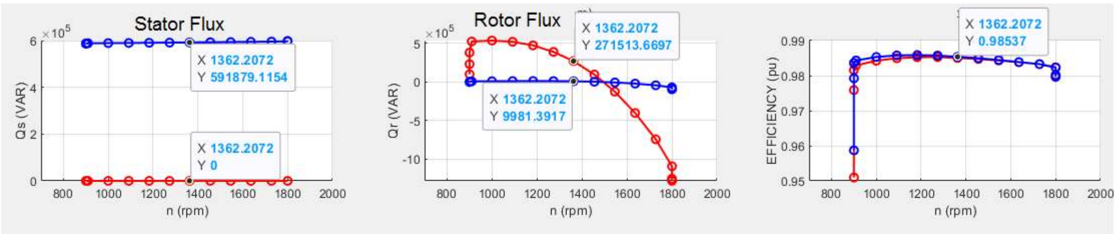

Figure 6.14 Flux related to the rotor and stator and the efficiency in the steady state behavior

After presenting the parameters related to the steady state behavior, our model in this case is operating at the rotational speed n = 1365 rpm as mentioned before. Therefore, we are comparing the values related to the theorical performance and modulation performance in the steady state.

The following Figure 6.15 shows the electromagnetic torque in the Simulink model which is equal to 6000 N.m

Therefore, the mechanical power can be computed as Equation (6.1):

$$P_{mec} = T_{em} * n = 857\ kW \tag{6.1}$$

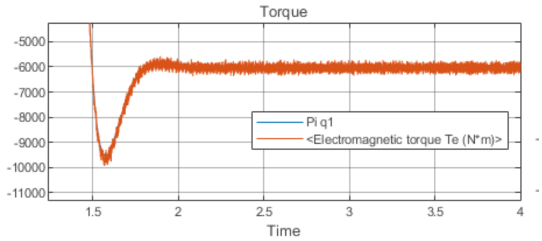

Figure 6.15 The electromagnetic torque in the Simulink model in steady state behavior

The following Figure 6.16 shows the rotor current in the Simulink model which is equal to: 1200 A and 0 A.

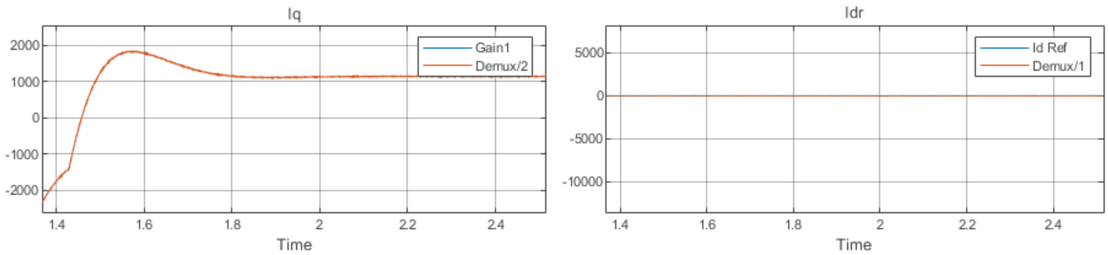

Figure 6.16 Rotor current in the Simulink model in steady state behavior

While the stator current in the Simulink model as shown in the Figure 6.17.

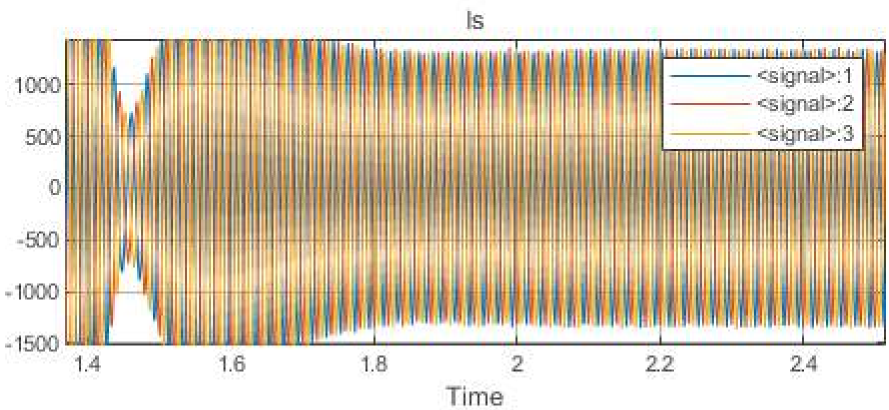

Figure 6.17 The stator current in the Simulink model in steady state behavior

The following Figure 6.18 shows the rotor voltage in the Simulink model which is equal to 55V.

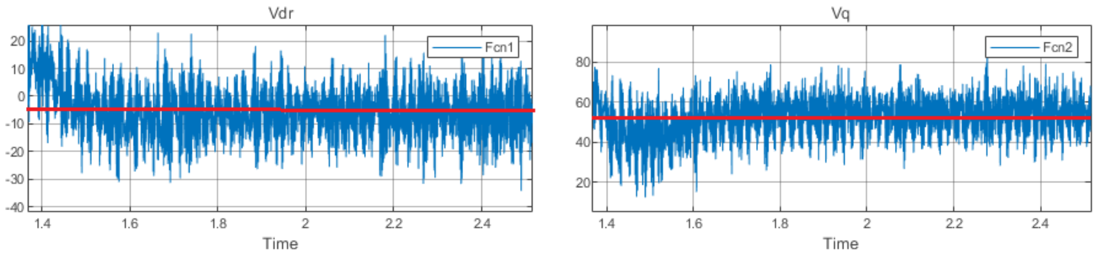

Figure 6.18 The rotor voltage in the Simulink model in steady state behavior

In the Table 6.1, we are summarizing the compared values related to the theorical performance and Simulink model in the steady state at the rotational speed n = 1365.

Table 6.1 Comparing values related to the theorical performance and Simulink model in the steady state at the rotational speed n = 1365

Parameters	**Steady State**	
	Theorical Values	Simulink model
Rotational speed (rpm)	1365	1365
Electromagnetic torque (N.m)	-6066	-6000
Mechanical power (kW)	853	857
Rotor current (A)	1160	1200
Stator current (A)	1116	1150
Rotor voltage (V)	54	55

6.3 Wind Turbine Model

As shown in the following Figure 6.19, the additional subsystem is the model of the wind turbine, while the input torque of the Asynchronous Machine is delivered from the wind turbine model.

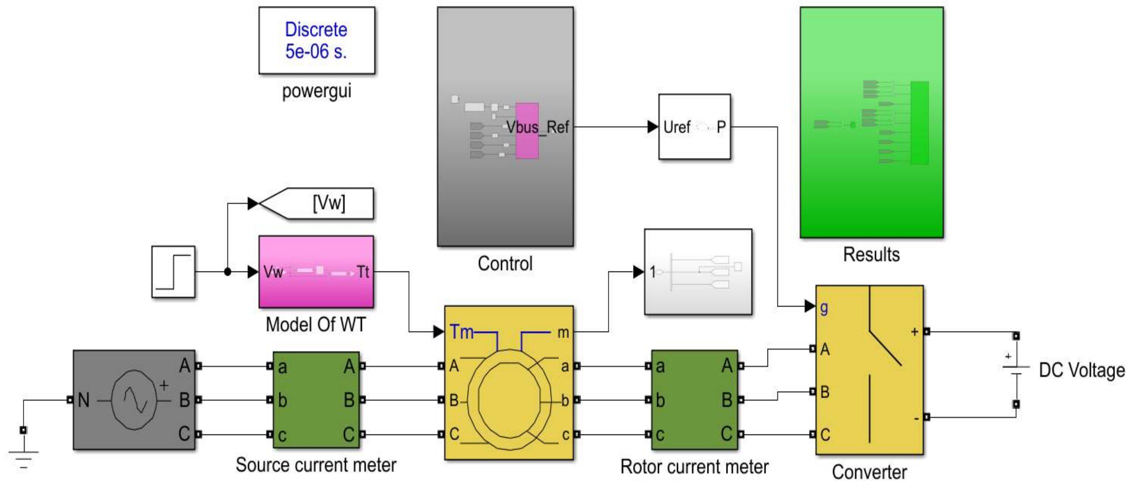

Figure 6.19 Block of wind turbine in the Simulink model

In the considered model of the wind turbine, the captured mechanical energy is transformed into electrical energy by means of the DFIG. Eventually, this electrical energy is delivered to the public grid or to network. The momentum theory is adopted in order to model the performance of the wind turbine. Regarding some ideal consideration and optimal assumptions, the captured energy can be expressed as shown before as Equation (6.2):

$$P_{mec} = \frac{1}{2}.(\rho.A_R.V^3).C_p(\beta,\lambda) \tag{6.2}$$

The following Figure 6.20 shows the adopted model of the wind turbine based on the previous theory. In addition, the captured torque is delivered by the gear box ratio.

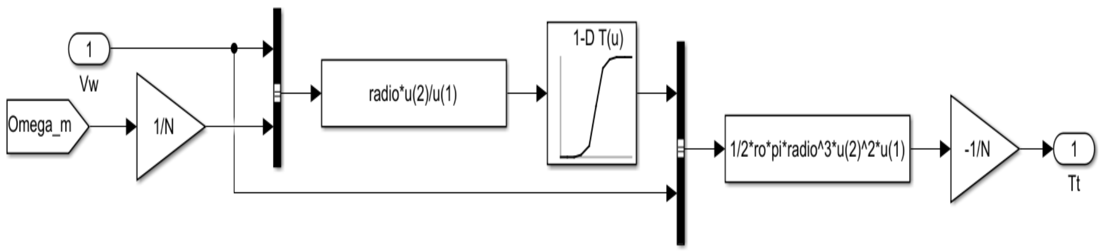

Figure 6.20 Adopted model of the wind turbine

According to the parameters and the coefficients which are adopted in our model, we are presenting here the performance curves related to the wind turbine model, as shown in the following Figure 6.21 for the C_p coefficient in terms of λ and the Figure 6.22 for the captured energy P_{mec} in terms of the speed.

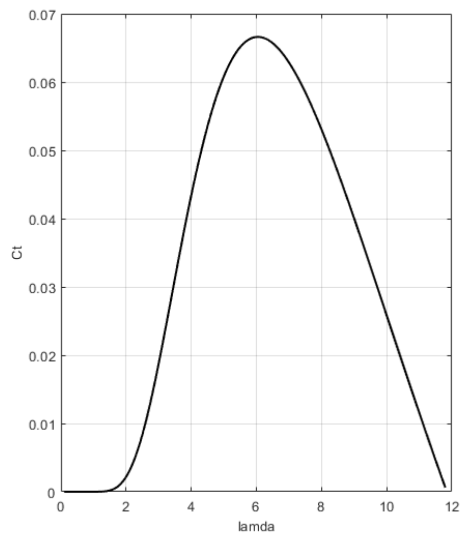

Figure 6.21 C_p coefficient in terms of λ

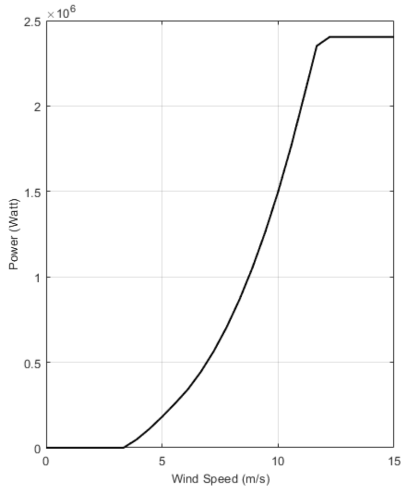

Figure 6.22 Captured energy $\boldsymbol{P_{mec}}$ in terms of the wind speed

In order to set the operating point, we are adopting the Maximum Power Point (MPP) method as shown in the Figure 6.23 which delivers the value of the C_p coefficient at maximum (i.e., C_{pmax}) at the optimal value of λ (i.e., λ_{opt})). Consequently, the captured energy becomes as Equation (6.3) and Equation (6.4):

$$\lambda_{opt} = \frac{\Omega_R}{V} r_R \quad \rightarrow \quad V = \frac{\Omega_R}{\lambda_{opt}} r_R \tag{6.3}$$

$$P_{mec} = \frac{1}{2}.\left(\rho.\pi(r_R^{\,2}).(\frac{\Omega_R}{\lambda_{opt}} r_R)^3\right).C_{pmax} = K_{opt} * \Omega_R^{\,3} \tag{6.4}$$

Where K_{opt} is the optimal coefficient which guarantees the MPP operating point and can be expressed as Equation (6.5):

$$K_{opt} = \frac{1}{2}.\left(\rho.\pi(r_R^{\,5}).(\frac{1}{\lambda_{opt}})^3 C_{pmax}\right) \tag{6.5}$$

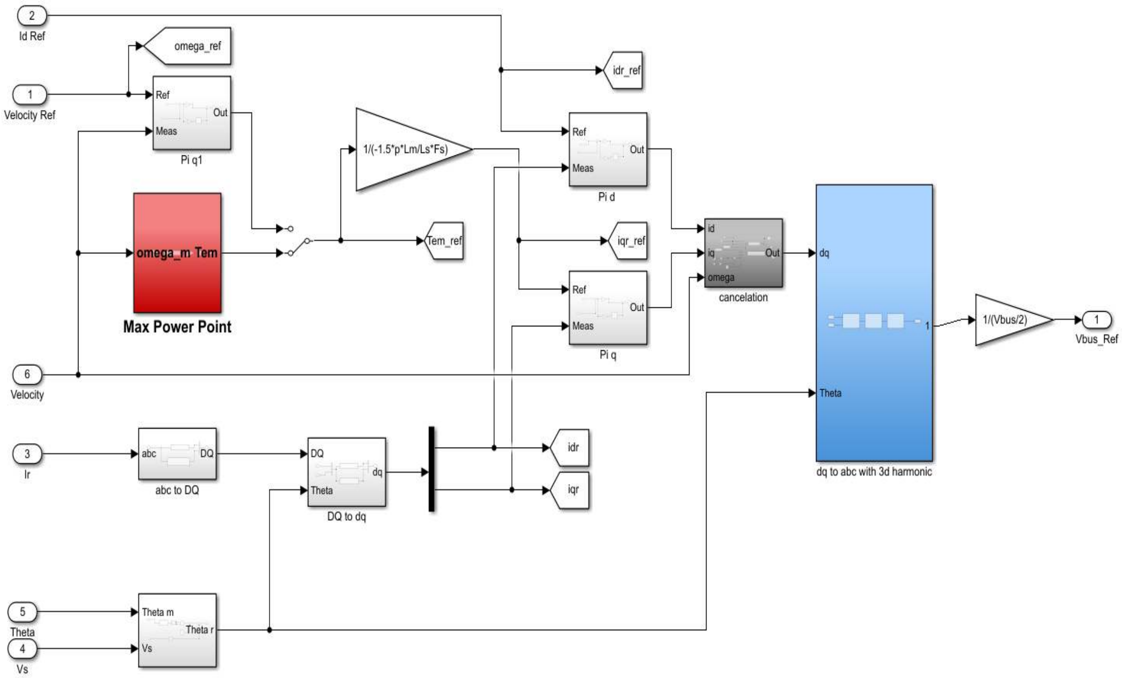

Figure 6.23 The Maximum Power Point (MPP) block

The following Figure 6.24 shows the most representative curves of the DFIG model based on the wind turbine model considering the MPP operating point at two speeds (speed of 170 m/sec at time 3 sec and speed of 205 m/sec at time 6 sec)

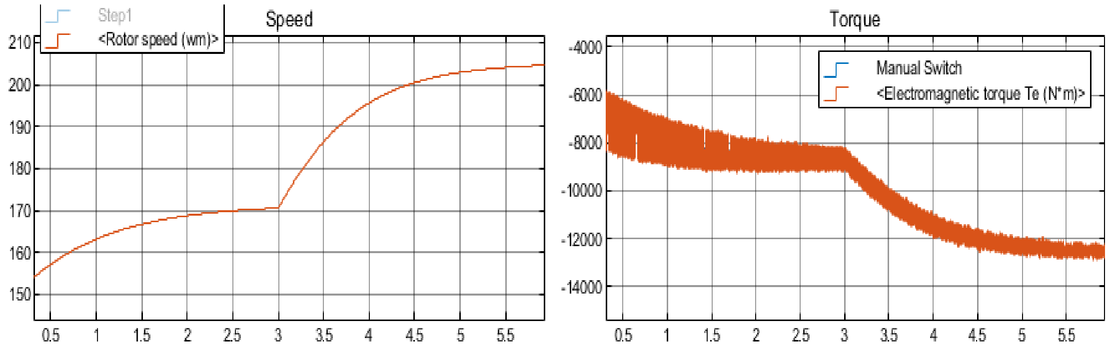

Figure 6.24 Speed and torque curves of the DFIG model based on the wind turbine model

We can observe that the control process is done without override and zero final error. The control loop is responsible for chasing the reference or objective speed even with the change in the value.

On the other hand, the control process of the current is done as shown in the following Figure 6.25, while the method of zero value of the d component related to the rotor current is adopted.

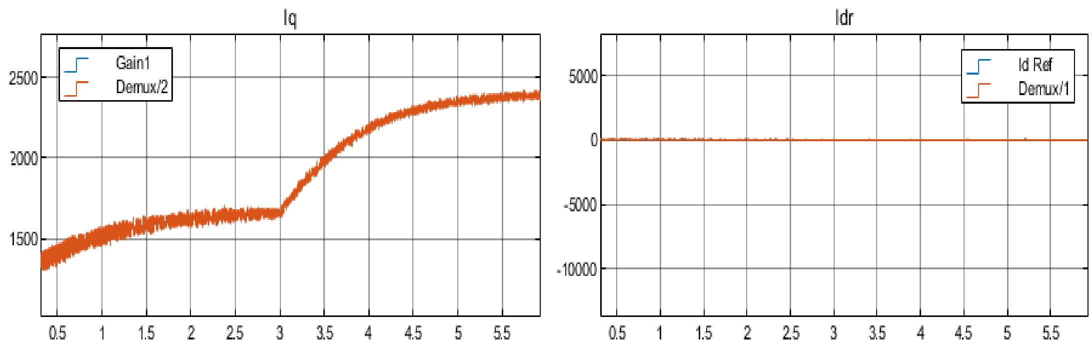

Figure 6.25 Rotor current curves of the DFIG model based on the wind turbine model

In addition, we are presenting the current of the rotor and stator according to the input step of the objective speed as illustrated in the following Figure 6.26. Referring to the transition phase, we note that an increase in the current of stator is exerted until it returns to its stable phase as long as the speed is constant.

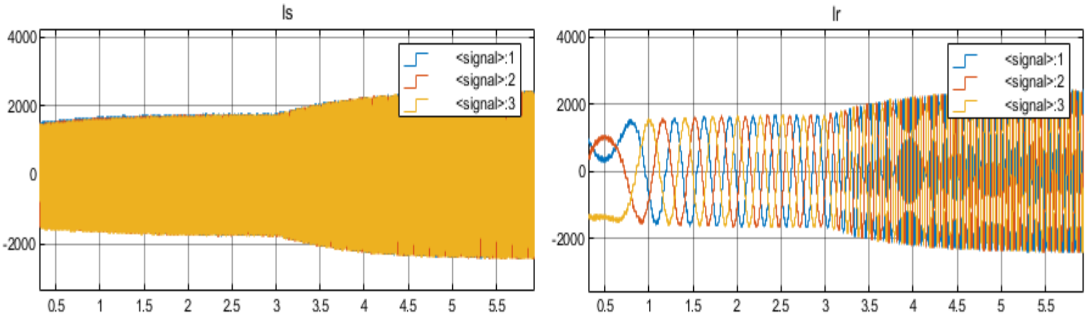

Figure 6.26 Rotor and stator current curves of the DFIG model based on the wind turbine model

We can observe in the transition phase and for the rotor current that at the synchronous speed, the current of rotor is developed a DC current which point to the synchronization phase in DFIG system.

6.4 Complete DFIG System

In this very step, we are modeling the complete model which includes the control loops of rotor current and DFIG connection beside the control loops of grid side. As shown in the following Figure 6.27, this overall system consists basically of the following main blocks:

- Three Phase Programmable Voltage Source.
- An Asynchronous Machine.
- Universal Bridge.
- Rotor Side Control Subsystem.
- Grid Side Control Subsystem.
- Rotor and Grid filters.
- Transformers.

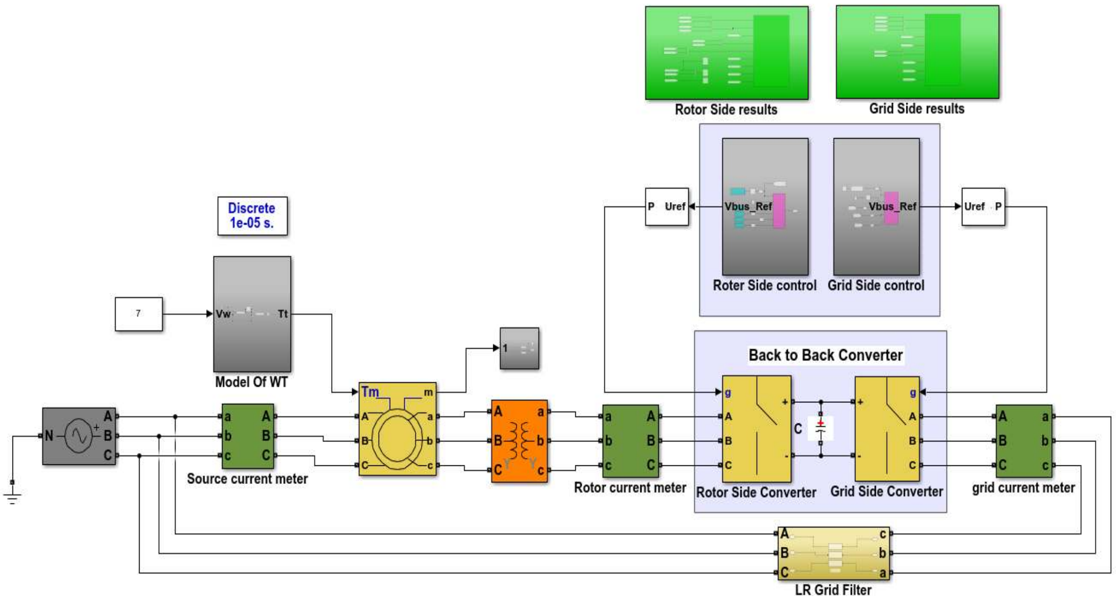

Figure 6.27 Control loops of rotor current and DFIG connection beside the control loops of grid side

We are presenting here, in this complete model, the input torque for the asynchronous machine as the resultant torque which comes from the wind turbine model. As shown in the following Figure 6.28, the acquisition block includes the output parameters (Rotor Angle Theta, Rotor Speed and Electromagnetic Torque) of the asynchronous machine which matter us and used in the Rotor Side Control Subsystem.

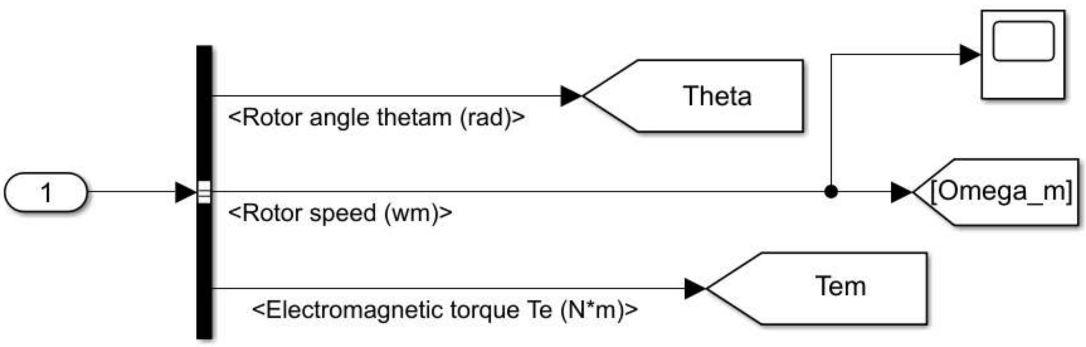

Figure 6.28 Acquisition block of asynchronous machine

The block where the control method is implemented is the Rotor Side Control Subsystem as shown in the following Figure 6.29. This block takes as an input the parameters; rotor speed, reference speed, estimated value of rotor current, rotor angle theta and source voltage) while the output is the voltage of Bus which is the input of the PWM generator. Eventually, we have to point to that the loops of control are applied regarding those currents of rotor are relative to the stator.

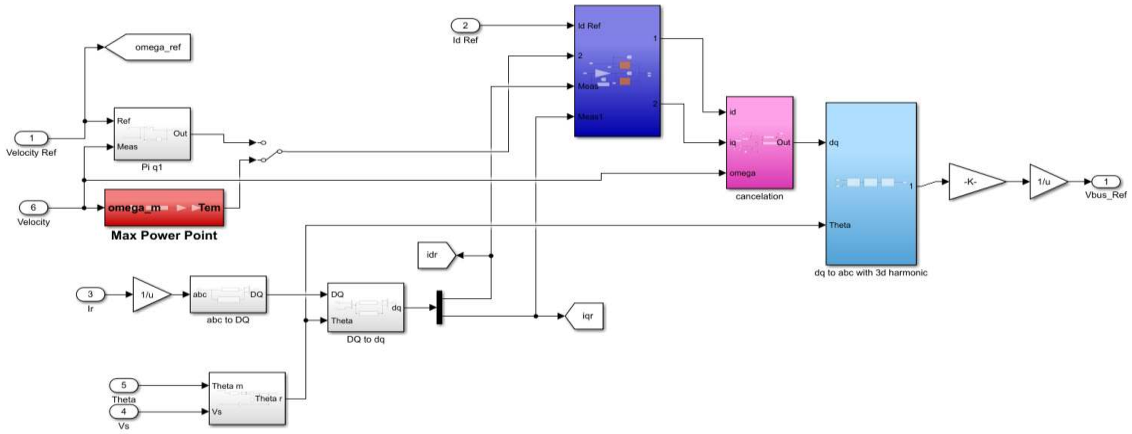

Figure 6.29 Rotor side control subsystem considering MPP method

This subsystem is the implementation of the Current Control Loop of the rotor side which is discussed before. Furthermore, we have to point here that all the values related to machine's parameters, PI regulator and references and correction values are set and adjusted in a MATLAB code file and linked to the Simulink model.

On the other hand, and in a similar way, the implementation of the Current Control Loop of the grid side is shown in the following Figure 6.30.

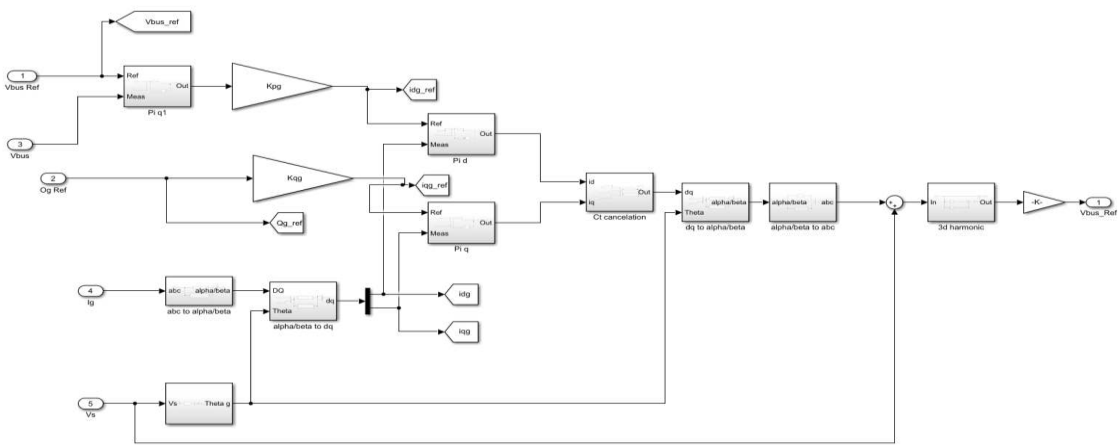

Figure 6.30 Grid side control subsystem

The three phases programmable voltage source is responsible for an input of 590-volt magnitude and 50Hz frequency as shown in the following Figure 6.31.

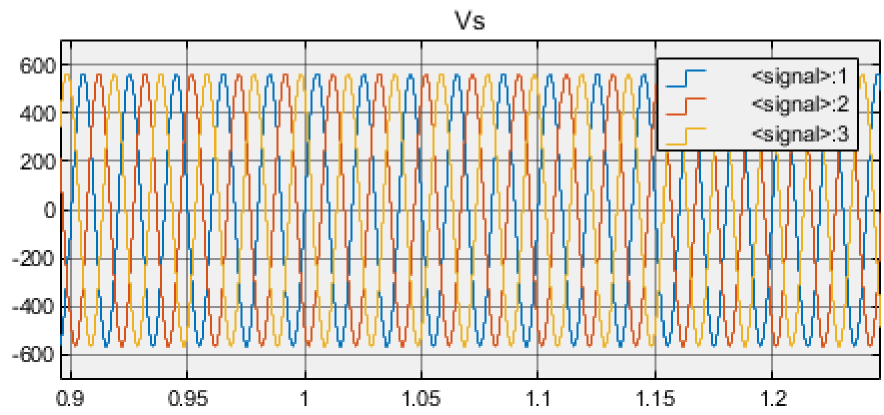

Figure 6.31 Input signal of three phases programmable voltage source

6.4.1 Rotor side performance

The reference or objective speed is entered as a ramp signal with an initial value of 0 m/sec and 147 m/sec as a final value as shown in the following Figure 6.32. According to the machine adopted, we computed the synchronous speed as 147 m/sec. In addition, we are presenting the torque signal as shown

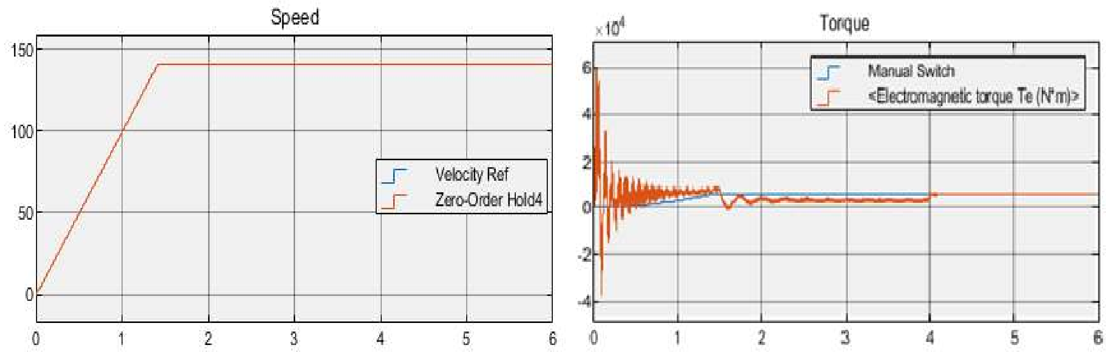

Figure 6.32 Speed and torque curves for the complete DFIG model

We can observe that the control process is done zero final error after the system is stable. The control loop is responsible for chasing the reference or objective speed even with the change in the value.

On the other hand, the control process of the current is done as shown in the following Figure 6.33, while the method of zero value of the d component related to the rotor current is adopted and implemented in the stable phase of the system.

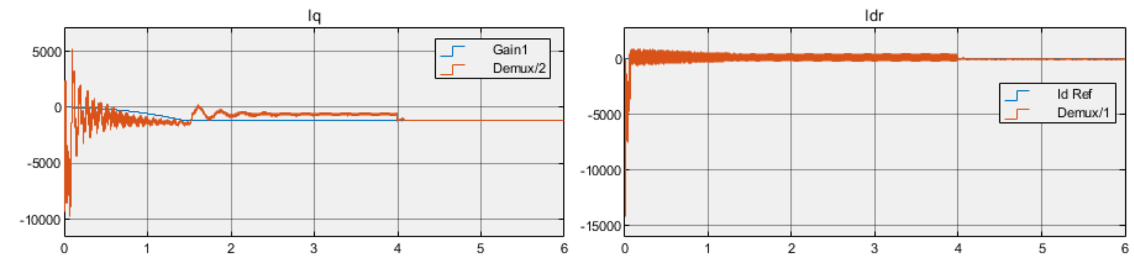

Figure 6.33 Rotor current components for the complete DFIG model

In addition, we are presenting the current of the rotor and stator according to the input step of the objective speed as illustrated in the following Figure 6.34. Referring to the transition phase, we note that an increase in the current of stator is exerted until it returns to its stable phase as long as the speed is constant.

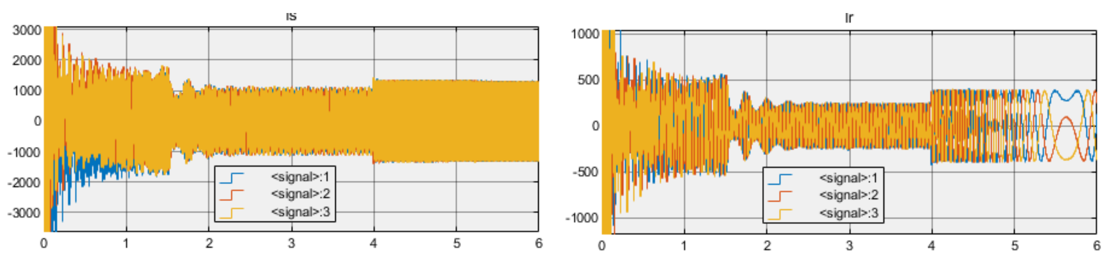

Figure 6.34 Rotor and stator current for the complete DFIG model

We can observe in the stale phase and for the rotor current that at the synchronous speed, the current of rotor is developing a DC current which point to the synchronization phase in DFIG system.

It worth to mention that we are neglecting the initial response at the beginning moment, because we are considering that the rotor and stator is connected permanently, while it is not the case in the real implementation. Therefore, a pick in all signals is exerted at the beginning moment as shown.

6.4.2 Grid side performance

The following Figure 6.35 illustrates the Controlled signal of the grid voltage beside the reference or objective signal which is considered as 1150 Volt.

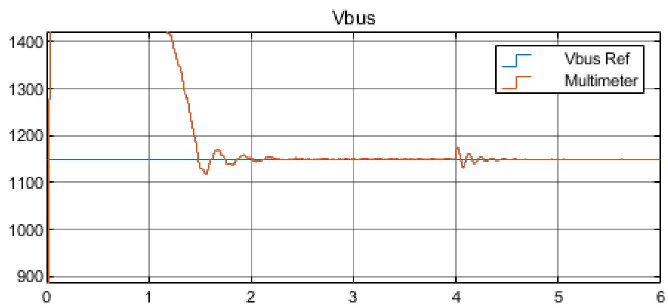

Figure 6.35 Controlled signal of the grid voltage beside the objective signal

We can observe that the control process is done with zero final error after the system is stable. The control loop is responsible for chasing the reference or objective grid voltage even with the change in the value. The following Figure 6.36 shows the constant vale of the reactive power related to the grid.

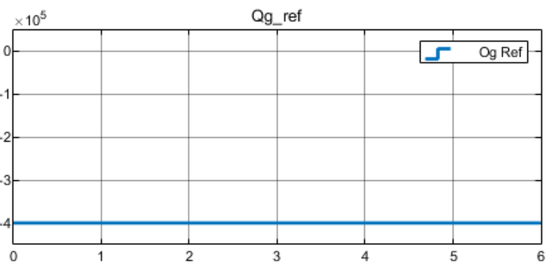

Figure 6.36 The constant vale of the reactive power related to the grid

The following Figure 6.37 shows the most representative curves of the DFIG model based on the wind turbine model related to grid side of the systems.

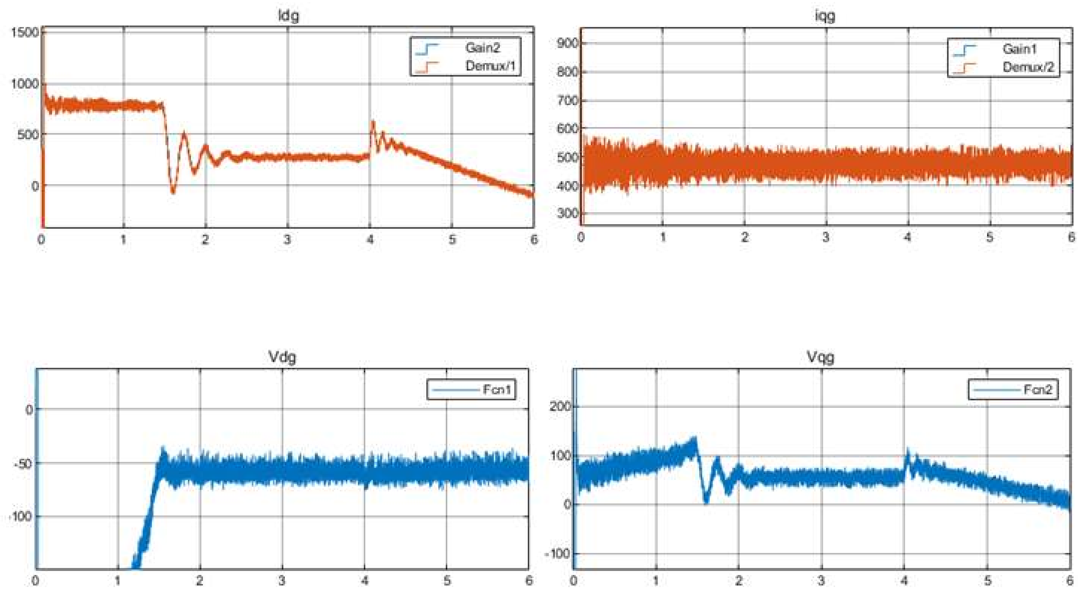

Figure 6.37 The most representative curves of the DFIG model based on the wind turbine model related to grid side

In addition, we are presenting the current of the grid according to the input step of the objective voltage as illustrated in the following Figure 6.38. Referring to the transition phase, we note that an increase in the current of stator is exerted until it returns to its stable phase as long as the speed is constant.

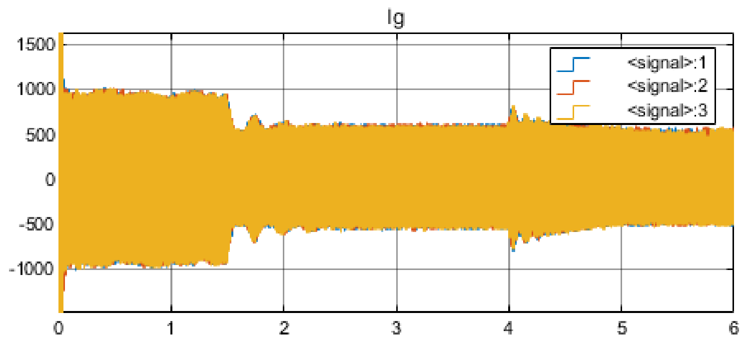

Figure 6.38 Current of the grid according to the input step of the objective voltage

6.5 Symmetrical Voltage Dips

The sudden drop in the voltage of the grid is known as a voltage dip. This drop may be caused by any error in the network. We are analyzing here a case of dealing with a

Symmetrical Voltage Dips; also, the behavior of the system will be addressed regarding the impact on the stator flux. In this very step, we are modeling crowbar protection which is responsible for dealing with the sudden drop in the voltage of the grid as shown in Figure 6.39.

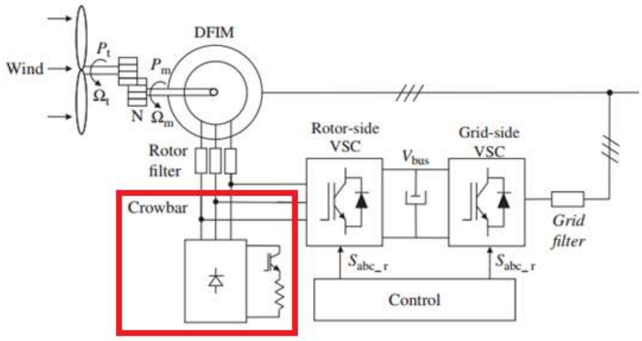

Figure 6.39 Modeling of crowbar protection (Pena et al. 1996)

In this very step, we are modeling the complete model which includes the control loops of rotor current and DFIG connection beside the control loops of grid side and the crowbar protection. As shown in the following Figure 6.40, this overall system consists basically of the main subsystems beside the additional ones:

- Universal Bridge.
- Ideal Switch.
- Protection Resistance.

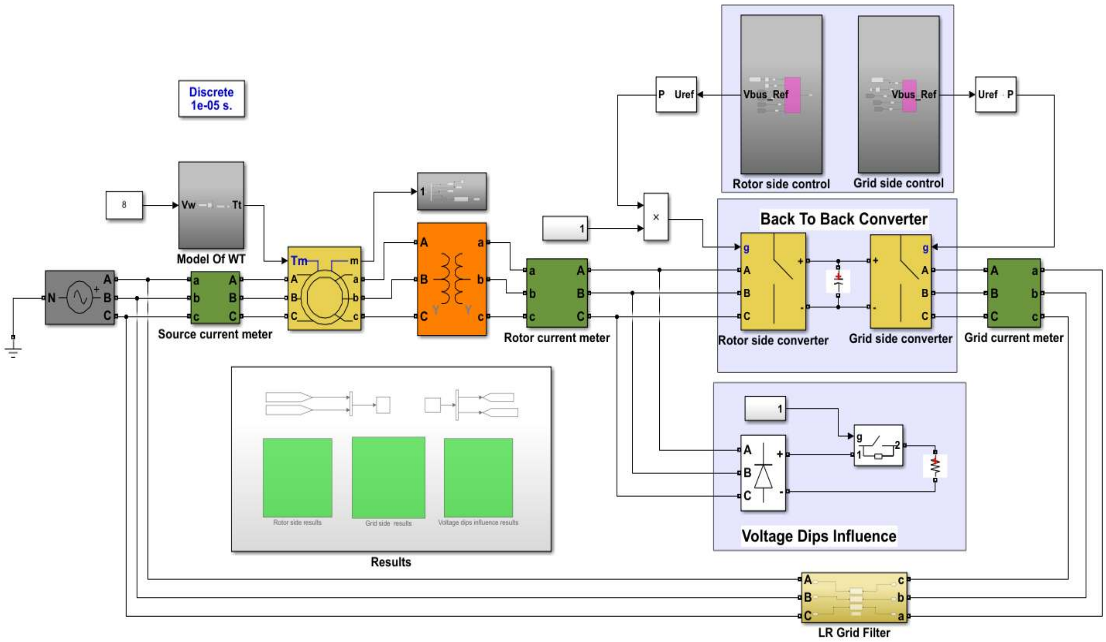

Figure 6.40 Overall system model beside the voltage dips block

The three phases programmable voltage source is responsible for an input of 590-volt magnitude and 50Hz frequency as shown in the following Figure 6.41. In addition, the voltage dip of 90% (sudden drop from 600 Volt to 60 Volt) is occurred at the time of 3 sec until the 3.5 sec, while the recovery phase is set as a ramp signal.

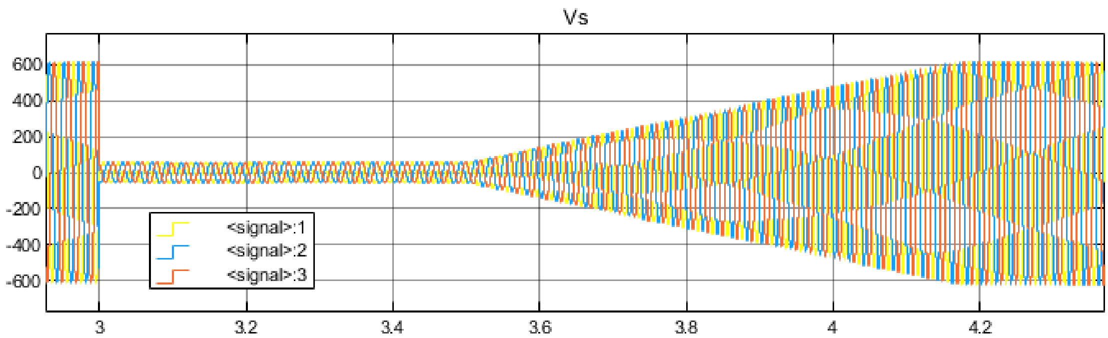

Figure 6.41 Voltage dips input signal

At the time of 3 sec, we can see that the current of the protection resistance is delivered a very high value in the current as a pick which remain for several cycles (0.1 sec) as shown in the following Figure 6.42.

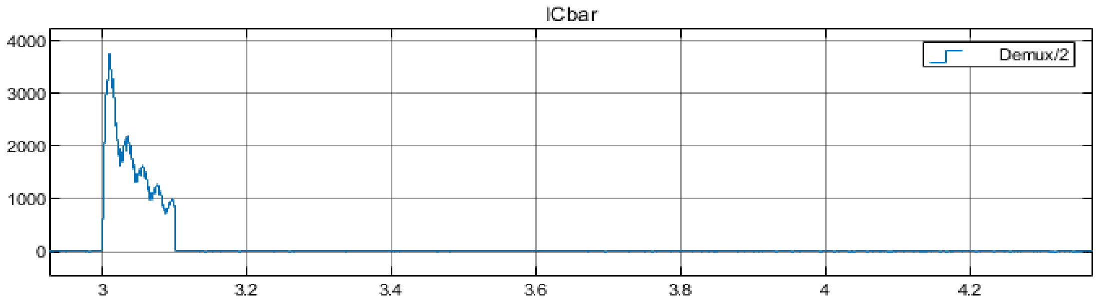

Figure 6.42 Current of the protection resistance

The following Figure 6.43 shows the most representative curves of the DFIG model based on the wind turbine model related to grid side of the systems.

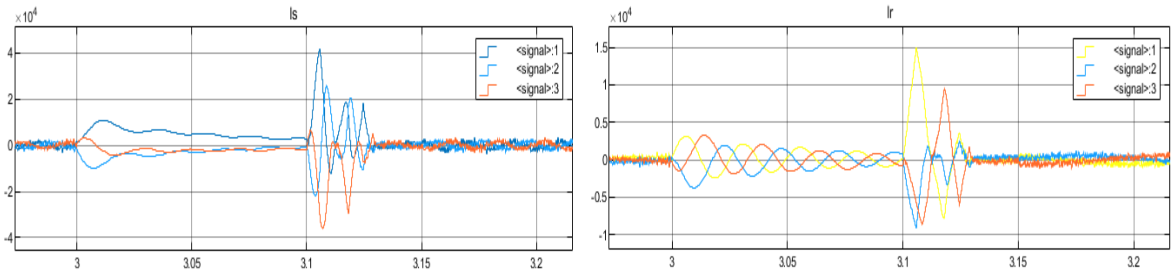

Figure 6.43 Current of rotor and stator curves of the DFIG model in voltage dips case

We can observe that during the protection phase, the current of the stator and rotor is experiencing a high value relative to the steady state values until the control is recovered and a new steady state is reached. The same case is delivered for the exerted torque as seen in Figure 6.44.

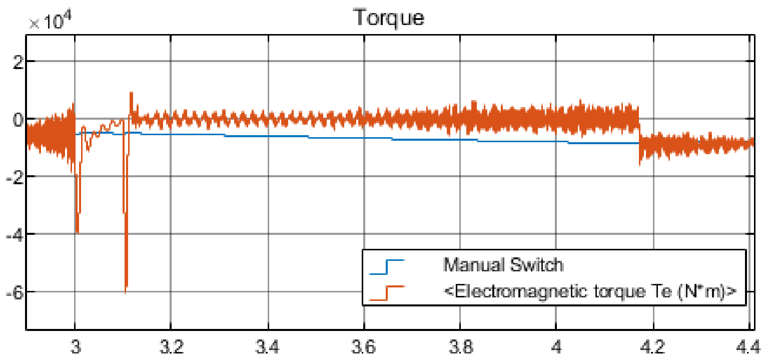

Figure 6.44 Torque of the DFIG model in voltage dips case

6.6 Dynamic Case

In order to implement the Dynamic Case, we are applying a step signal of the reactive and then evaluate the performance of the DFIG system as shown in Figure 6.45.

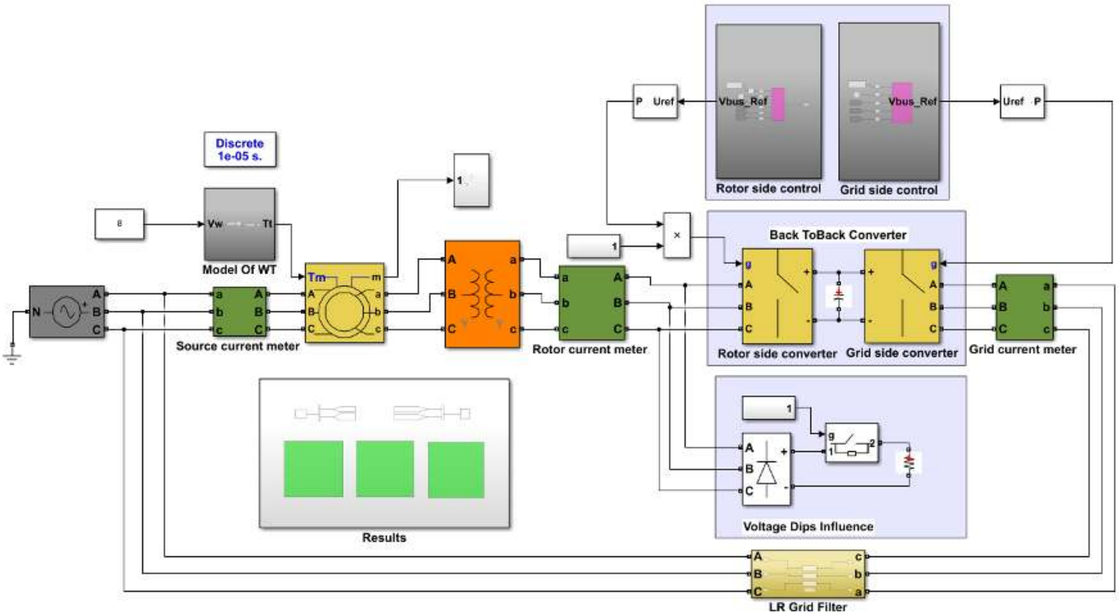

Figure 6.45 DFIG model in dynamic case

The following Figure 6.46 shows the input signal of grid reactive power of initial value of zero and final one of 150 kW which occurs at time of 2.5 sec.

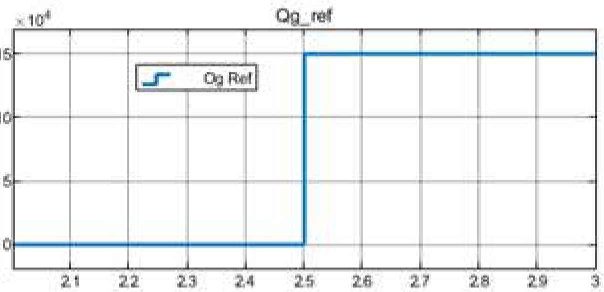

Figure 6.46 Input signal of grid reactive power

The following Figure 6.47 shows the most representative curves of the DFIG model based on the wind turbine model related to Dynamic Case.

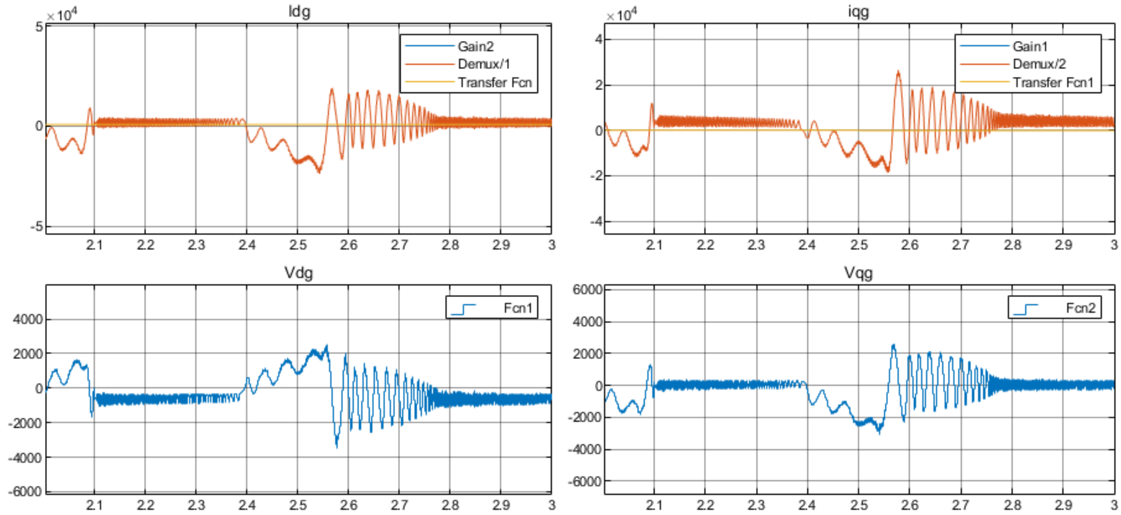

Figure 6. 47 Most representative curves of the DFIG model in dynamic case

We can see that the current and voltage of the grid experience a transition phase in the moment of the step until they reach the recovery point and settle down at the steady state again.

7. CONCLUSION AND RECOMMENDATION

In this thesis, we have implemented and analyzed the previous theoretical concepts of controlling DFIG systems. The implementation has done through sequential steps and subsystems in order to implement the complete controlling systems while various issues have been evaluated and discussed through the modulation process. Furthermore, the modulation process has been carried out based on MATLAB/ Simulink environment.

We observed that the control process is done with 0.15-time response and 2.5% override and zero final error. The control loop was responsible for chasing the reference or objective speed even with the change in the value. In the transition phase and for the rotor current at the synchronous speed, the current of rotor has developed a DC current which point to the synchronization phase in DFIG system neglecting the initial response at the beginning moment.

The Implementation of the DFIG System (Control loops of rotor current, DFIG connection) has been done considering the evaluation of Steady State Case. For evaluation purpose, a random operating point has been considered and the corresponding values and parameters have been compared between the theoretical model and DFIG model. The compared values related to the theorical performance and Simulink model in the steady state at the rotational speed $n = 1365$.

Table 6.2 Error in computed value of various parameters related to DFIG system

Parameters	Steady State		Error %
	Theorical Values	Simulink model	
Rotational speed (rpm)	1365	1365	0
Electromagnetic torque (N.m)	-6066	-6000	1.1
Mechanical power (kW)	853	857	0.47
Rotor current (A)	1160	1200	3.3
Stator current (A)	1116	1150	2.95
Rotor voltage (V)	54	55	1.8

The Implementation of Wind Turbine Model has been performed and linked to the DFIG systems, while the Maximum Power Point (MPP) method is adopted considering the optimal coefficients which are computed and adjusted in model. While implementation of the overall DFIG System (Control loops of rotor and grid sides, DFIG connection, Wind Turbine Model) has been achieved with the Back-to-Back Converter.

Finally, the Symmetrical Voltage Dips has been evaluated and addressed using protection subsystems, while the results showed that the system has reached a new steady state point after several cycles (within 0.1 sec of cycles).

Speaking of recommendation related to this thesis which can be titled as future work, there are some interesting aspects which may be considered in a future work, such as:

- Evaluation of Unsymmetrical Voltage Dips.
- Evaluation of Frequency Dips in the voltage of Grid.
- Evaluation of Harmonics in voltage.

REFERENCES

Abad, G., Rodriguez, J., Marroyo, M. and Iwanski, G. 2011. Doubly fed induction machine: modeling and control for wind energy generation applications, Wiley-IEEE Press, 619 pages, New Jersey.

Abu-Rub, H., Malinowski, M. and Al-Haddad, K. 2014. Power electronics for renewable energy systems, transportation and industrial applications, John Wiley & Sons Ltd, 726 pages, West Sussex.

Ackermann, T. and Söder, L. 2002. An overview of wind energy-status 2002, Renewable and Sustainable Energy Reviews, 6(1–2): 67–127.

Boldea, I. and Nasar, S. A. 2016. Electric drives, CRC press, 636 pages, New York

Burton, T., Sharpe, D., Jenkins, N. and Bossanyi, E. 2001a. Wind Energy Handbook, John Wiley & Sons Ltd, 733 pages, West Sussex.

Carlson, O., Hylander, J. and Thorborg, K. 1996. Survey of variable speed operation of wind turbines, In Proc. of EUWEC, Bedford, 406-409.

Datta, R. and Ranganathan, V. T. 2002. Variable-speed wind power generation using doubly fed wound rotor induction machine-a comparison with alternative schemes, IEEE Transactions on Energy Conversion, 17(3): 414–421.

Geng, H., Liu, C. and Yang, G. 2012. LVRT capability of DFIG-based WECS under asymmetrical grid fault condition. IEEE Transactions on Industrial Electronics, 60(6): 2495–2509.

Döşoğlu, M. K. (2021). Hybrid control approach for low-voltage ride-through capability in doubly-fed induction generator-based wind turbines. Computers &Electrical Engineering, 90, 106972.

Gebru, F. M., Khan, B., & Alhelou, H. H. (2020). Analyzing low voltage ride through capability of doubly fed induction generator based wind turbine. Computers & Electrical Engineering, 86, 106727.

Grauers, A. 1994. Synchronous generator and frequency converter in wind turbine applications: system design and efficiency, Technical Report No 175L, Chalmers University of Technology, 124 pages, Göteborg.

Hansen, L. H., Helle, L., Blaabjerg, F., Ritchie, E., Munk-Nielsen, S., Bindner, H., Soerensen, P. and Bak-Jensen, B. 2001. Conceptual survey of generators and power electronics for wind turbines, Pitney Bowes Management Services, 95 pages, Roskilde.

Harnefors, L. 2002. Control of Variable Speed Drives; Applied Signal Processing and Control, Mälardalen University, 195 pages, Västeras.

Heller, M. and Schumacher, W. 1997. Stability analysis of doubly-fed induction machines in stator flux reference frame, European Conference on Power Electronics and Applications, 2: 2–707.

Ioannides, M. G. and Tegopoulos, J. A. 1988. Optimal efficiency slip-power recovery drive, IEEE Transactions on Energy Conversion, 3(2): 342–348.

Johnson, G. L. 1985. Wind energy systems, Prentice Hall Press, 348 pages. New Jersey.

Larsson, Å., Sørensen, P. and Santjer, F. 1999. Grid impact of variable-speed wind turbines, European wind energy conference, Nice, 225-228.

Leonhard, W. 2001. Control of electrical drives, Springer Science & Business Media, 455 pages, Berlin.

Liserre, M., Cardenas, R., Molinas, M. and Rodriguez, J. 2011. Overview of multi-MW wind turbines and wind parks, IEEE Transactions on Industrial Electronics, 58(4): 1081–1095.

Mehrjerdi, H., Hemmati, R., Shafie-khah, M., & Catalão, J. P. S. (2021). Zero Energy Building by Multicarrier Energy Systems including Hydro, Wind, Solar, and Hydrogen. IEEE Transactions on Industrial Informatics, 17(8), 5474–5484.

Morel, L., Godfroid, H., Mirzaian, A. and Kauffmann, J. M. 1998. Double-fed induction machine: converter optimization and field-oriented control without position sensor, IEE Proceedings-Electric Power Applications, 145(4): 360–368.

Mostafa Nosratabadi, S., Hemmati, R., Bornapour, M., & Abdollahpour, M. (2021). Economic evaluation and energy/exergy analysis of PV/Wind/PEMFC energy resources employment based on capacity, type of source and government incentive policies: Case study in Iran. Sustainable Energy Technologies and Assessments, 43, 100963.

Mutschler, P. and Hoffmann, R. 2002. Comparison of wind turbines regarding their energy generation, 2002 IEEE 33rd Annual IEEE Power Electronics Specialists Conference. Proceedings (Cat. No. 02CH37289), 1: 6–11.

Nosratabadi, S. M., Hemmati, R., & Khajouei Gharaei, P. (2021). Optimal planning of multi-energy microgrid with different energy storages and demand responsive loads utilizing a technical-economic-environmental programming. International Journal of Energy Research, 45(5), 6985–7017.

Papadopoulos, M. P. 1999. Voltage quality change by grid-connected wind turbines, European Wind Energy Conference, Nice, France, 1999, 783–785.

Pena, R., Clare, J. C. and Asher, G. M. 1996. Doubly fed induction generator using back-to-back PWM converters and its application to variable-speed wind-energy generation, IEE Proceedings-Electric Power Applications, 143(3): 231–241.

Petersson, A. 2005. Analysis, modeling and control of doubly-fed induction generators for wind turbines, PhD. Thesis, Chalmers University of Technology, 166 pages, Göteborg.

Petru, T. and Thiringer, T. 2000. Active flicker reduction from a sea-based 2.5 MW wind park connected to a weak grid, 2000 Nordic Workshop on Power and Industrial Electronics (NORpie 2000), Aalborg, Denmark, 256-262.

Qiao, W. and Harley, R. G. 2008. Improved control of DFIG wind turbines for operation with unbalanced network voltages, 2008 IEEE Industry Applications Society Annual Meeting, 1–7.

Rabelo, B. and Hofmann, W. 2001. Optimal active and reactive power control with the doubly-fed induction generator in the MW-class wind-turbines, 4th IEEE International Conference on Power Electronics and Drive Systems. IEEE PEDS 2001-Indonesia. Proceedings (Cat. No. 01TH8594), 1: 53–58.

Spera, D. A. 1994. Introduction to modern wind turbines, Wind Turbine Technology: Fundamental Concepts of Wind Turbine Engineering, 47–72.

Tang, Y. and Xu, L. 1995. A flexible active and reactive power control strategy for a variable speed constant frequency generating system, IEEE Transactions on Power Electronics, 10(4): 472–478.

Veers, P.S. 1988. Three-dimensional wind simulation. Sandia National Labs., Albuquerque, NM (USA). 36 pages.

Wang, S. and Ding, Y. 1993. Stability analysis of field oriented doubly-fed induction machine drive based on computer simulation. Electric Machines and Power Systems, 21(1): 11–24.

Winkelaar, D. 1991. Fast three-dimensional wind simulation and the prediction of stochastic blade loads, Tenth ASME Wind Energy Symposium, Houston, TX. 28-36.

Xu, L. and Cheng, W. 1995. Torque and reactive power control of a doubly fed induction machine by position sensorless scheme. IEEE Transactions on Industry Applications, 31(3): 636–642.

Zinger, D. S. and Muljadi, E. 1997. Annualized wind energy improvement using variable speeds. IEEE Transactions on Industry Applications, 33(6): 1444–1447.

CURRICULUM VITAE

Personal Information

Name and Surname : Abdullah Muwafaq Othman ALYOUSUF

Education

MSc	Çankırı Karatekin University Graduate School of Natural and Applied Sciences Department of Electrical and Electronics Engineering	2020-Present
Undergraduate	Al-Hadba University College Faculty of Engineering Department of Computer Technology Engineering	2012-2017

Work Experience

Year	**Institution**	**Position**
------	------------	------------